

Article

Wearable Sensors for Athletic Performance: A Comparison of Discrete and Continuous Feature-Extraction Methods for Prediction Models

Mark White ^{1,*} , Beatrice De Lazzari ^{2,3,4} , Neil Bezodis ¹  and Valentina Camomilla ^{2,4} 

- ¹ Applied Sports, Technology, Exercise and Medicine (A-STEM) Research Centre, Faculty of Science and Engineering, Swansea University, Swansea SA2 8PP, UK
- ² Department of Movement, Human and Health Science, University of Rome "Foro Italico", 00135 Rome, Italy
- ³ GoSport s.r.l., Via Basento, Lazio, 00198 Roma, Italy
- ⁴ Interuniversity Centre of Bioengineering of the Human Neuromusculoskeletal System, University of Rome "Foro Italico", 00135 Rome, Italy
- * Correspondence: m.g.e.white@swansea.ac.uk

Abstract: Wearable sensors have become increasingly popular for assessing athletic performance, but the optimal methods for processing and analyzing the data remain unclear. This study investigates the efficacy of discrete and continuous feature-extraction methods, separately and in combination, for modeling countermovement jump performance using wearable sensor data. We demonstrate that continuous features, particularly those derived from Functional Principal Component Analysis, outperform discrete features in terms of model performance, robustness to variations in data distribution and volume, and consistency across different datasets. Our findings underscore the importance of methodological choices, such as signal type, alignment methods, and model selection, in developing accurate and generalizable predictive models. We also highlight the potential pitfalls of relying solely on domain knowledge for feature selection and the benefits of data-driven approaches. Furthermore, we discuss the implications of our findings for the broader field of sports biomechanics and provide practical recommendations for researchers and practitioners aiming to leverage wearable sensor data for athletic performance assessment. Our results contribute to the development of more reliable and widely applicable predictive models, facilitating the use of wearable technology for optimizing training and enhancing athletic outcomes across various sports disciplines.

Keywords: accelerometer; countermovement jump; feature extraction; functional principal component analysis; inertial measurement units; jump power; signal alignment; smartphone; sport; wearables

MSC: 92C10; 62-08; 62J05; 62J07



Citation: White, M.; De Lazzari, B.; Bezodis, N.; Camomilla, V. Wearable Sensors for Athletic Performance: A Comparison of Discrete and Continuous Feature-Extraction Methods for Prediction Models. *Mathematics* **2024**, *12*, 1853. <https://doi.org/10.3390/math12121853>

Academic Editor: Daniel-Ioan Curiaç

Received: 15 April 2024

Revised: 7 June 2024

Accepted: 8 June 2024

Published: 14 June 2024



Copyright: © 2024 by the authors. Licensee MDPI, Basel, Switzerland. This article is an open access article distributed under the terms and conditions of the Creative Commons Attribution (CC BY) license (<https://creativecommons.org/licenses/by/4.0/>).

1. Introduction

Wearable sensors have become commonplace in sport, ranging from mass participation events to high-level competitions. Given the practicality and convenience of using them in the field, wearable sensors have numerous potential sporting applications, providing valuable feedback to users and researchers alike [1–3]. Data from wearable sensors are becoming increasingly used in machine-learning models in attempts to predict output variables of interest, such as performance metrics or potential injury risk factors [4,5]. However, the methods for processing and analyzing sensor data vary widely across the literature [4,6–8].

Feature extraction is essential when using wearable sensor data as inputs to machine-learning models. This process is necessary to reduce data dimensionality while retaining signal characteristics that contain information deemed relevant to the application of interest [5,9]. In early force platform-based studies of vertical jumping, discrete features

were extracted from the ground reaction force–time–history using domain expertise in attempts to understand the factors influencing jump performance [10,11]. Later studies have progressed to extracting continuous features, typically determined by data-driven discovery techniques such as functional principal component analysis (FPCA) [12–14]. This gradual shift towards analyses that consider continuous features is purported to provide model inputs that comprise a more comprehensive description of the underlying signal. However, given the widely varying approaches in the literature, particularly when wearable sensors are used to provide these input signals, it remains unclear whether the complexity and time entailed in the continuous approach provide additional value beyond the use of discrete features, especially when the interpretation of continuous features can sometimes be challenging.

One previous study compared discrete with continuous features extracted from vertical ground reaction force (VGRF) data when estimating jump height [15] and found that continuous features from FPCA tended to yield a better estimation. However, this potentially favored the functional principal components (FPCs), as they were proportional to the area under the force–time curve and, therefore, directly related to the jump height, given the conservation of momentum. Wearable sensors also provide a different challenge as they typically yield the kinematics of a single sensor at a specific anatomical location. In addition, the sensor attachment method, location, and the likely changing orientation of the sensor throughout a movement may also make extracting relevant information from the signal more challenging. It is, therefore, essential to compare and contrast the efficacy of discrete and continuous features obtained from wearable sensor signals as inputs to ML models for such applications.

To assess the relative merits of using discrete or continuous features as inputs to ML models, we must also consider the interaction with other methodological decisions [16]. For example, certain model types may better suit different feature-extraction methods, while data volume and the distributions of the extracted features may also be important factors given the often opportunistic or limited samples obtained in applied sporting studies. Other considerations include the sensor type (e.g., IMU vs. accelerometer), the different locations for placement (e.g., handheld vs. trunk mounted), or other aspects [2,17].

To better understand these factors, a relatively simple, standardized sporting movement that is well understood is required. The countermovement jump (CMJ) offers a suitable choice as it has been studied extensively and is widely used for assessment in sports biomechanics and applied practice [18,19]. While the CMJ provides an exemplar to illustrate the key concepts studied in this paper, the findings have implications for the broader field, including the study of related athletic movements, signal processing techniques, and ML models, to name a few.

This study will systematically apply rigorous and robust methods for all stages of the modeling process to offer a deeper understanding of how different feature-extraction approaches can influence model performance. It aims to explore how different feature-extraction techniques influence wearable sensor-based models of CMJ performance while also considering the effect of other common methodological factors such as sampling, data collection, and model selection. More specifically, we set out to answer the following research questions.

1. Feature-extraction efficacy: How do discrete and continuous feature-extraction methods compare when modeling athletic performance metrics, such as the peak power output in the CMJ?
2. Model robustness: How robust are different model types, based on discrete or continuous features, or combinations of both, to variations in data distribution and sample size?
3. Generalizability: How consistent are the findings between studies where different sensors, placements, and/or data-collection protocols are used?

2. Methods

We developed a specific workflow to answer these questions (Figure 1). Data for our analysis was taken from two independent studies investigating the efficacy of using wearable inertial sensors to estimate vertical jump performance [20,21] (Table 1). Both investigations involved healthy sports science students, free of injury, all of whom had given their prior written consent. The studies were approved by the governing institutions' ethics committees, and further analysis of the data was conducted. Having two datasets was intended to allow for differences in sensor type and placement (research question 3) and make for a more thorough evaluation of the first two research questions. Full details of the data collection are available in the respective papers. We summarize the key information in Table 1 for convenience.

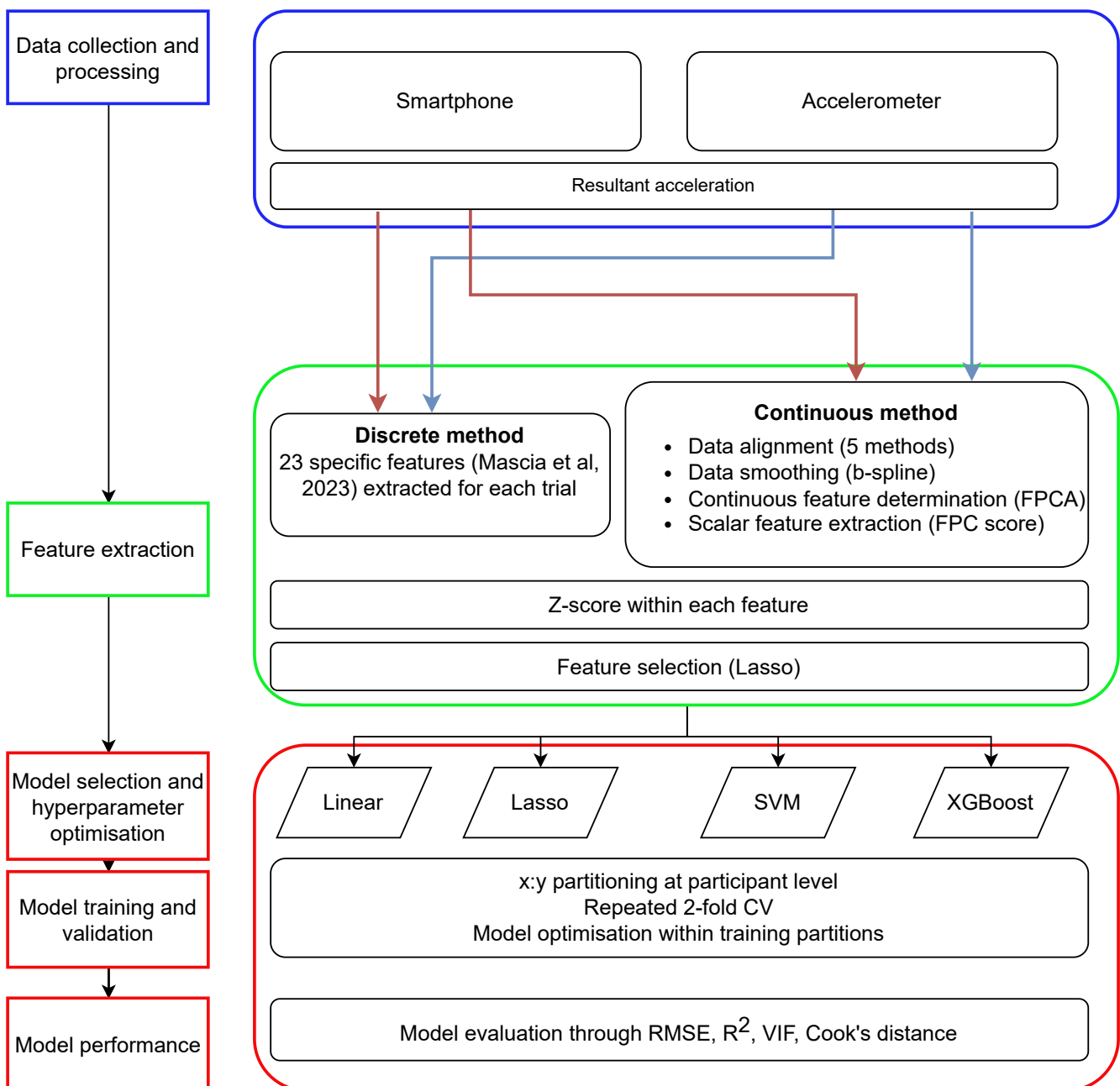


Figure 1. The workflow to address the three research questions. The left-hand side of the figure presents the general steps, while the right-hand side details the choices based on the available data [20].

Table 1. Experimental details of the two data collections used in this analysis: Smartphone data from Mascia et al., 2023 [20]; Accelerometer data from White et al., 2022 [21].

	Smartphone	Accelerometer
Participants	22 males, 10 females	48 males, 25 females *
Age (mean \pm SD)	26.5 \pm 4.1 years	21.6 \pm 3.3 years
Height (mean \pm SD)	1.74 \pm 0.08 m	1.75 \pm 0.10 m
Mass (mean \pm SD)	70.0 \pm 10.9 kg	71.2 \pm 15.1 kg
Device	Redmi 9T phone	Trigno sensor
Manufacturer	Xiaomi Technology, Beijing, China	Delsys Inc., Natick, MA, USA
Sampling Frequency	128 Hz	250 Hz
Onboard Sensors	Accelerometer: \pm 8 g; Gyroscope: \pm 360 deg/s	Accelerometer \pm 9 g
Placement	Handheld at sternum level	Taped to lower back (L4)
Reference force platform	Bertec	9260AA
Manufacturer	AMTI, Watertown, MA, USA	Kistler, Winterthur, Switzerland
Sampling Frequency	1000 Hz	1000 Hz
Valid jumps included	119	347
Peak Power (W/kg) †	40.7 \pm 8.9	45.1 \pm 7.6
Signal for Analysis	Resultant Acceleration	Resultant Acceleration

* The numbers of participants differ from those reported in the original study because we combined training and test datasets for this investigation. † Ground truth determined from vertical ground reaction force measured by a force plate.

2.1. Data Collections

The first study (“Smartphone” [20]) recruited 32 participants and gathered data from sensors onboard a Xiaomi Redmi 9T smartphone (triaxial accelerometer and gyroscope), handheld close to the chest at sternum level throughout each trial. The participants performed three or five CMJs for a total of 119 jumps. The second study (“Accelerometer” [21]) recruited 73 participants and employed a Delsys Trigno sensor containing only a triaxial accelerometer attached to the lower back with surgical tape. Most participants performed four valid CMJs, but 14 made eight jumps in total, having attended two rounds of data collection. One jump was rejected as invalid during processing, leaving 347 jumps in total. In both datasets, the time series encompassed the entire takeoff, flight, and landing phases.

As the Accelerometer dataset lacked the gyroscope data possessed by the Smartphone dataset, we used the resultant acceleration from both datasets, also making the analysis more robust to different sensor attachments [9]. This approach also made the input signals directly comparable. Hence, differences between the Smartphone and Accelerometer datasets were limited to the sensor make and placement.

We chose the mass-normalized peak external power output as our jump performance measure, given its common usage in elite sports alongside jump height, to monitor athlete training status and progression [19,22–24]. The external mechanical power is the product of the instantaneous force and the center of mass velocity. The ground truth for this metric was computed from the vertical ground reaction force recorded by a force plate in accordance with the recognized gold standard method [25].

2.2. Discrete Feature Extraction

Twenty-three discrete features devised by Mascia et al. [20] were used in the current study, as detailed in Appendix A.1. These included maxima, minima, gradients, and phase durations and tended to be informed by domain-specific knowledge. A complete list of features with their definitions is given in Appendix A.1. We did not include the three features based on variational mode decomposition (VMD) [26] used by Mascia et al. [20] because they were continuous features. However, we did include the VMD features in a combined feature set in the final part of the investigation, as described below in Section 2.4.

The discrete features were extracted from the resultant acceleration time series, and two series were derived from it, as described below. The resultant acceleration time series from the sensor were low-pass filtered using a 50 Hz 6th-order Butterworth filter, and after the gravitational acceleration was subtracted. (The gravitational offset was analogous to that performed on VGRF jump data, which has the participant's bodyweight subtracted to yield the net force acting on the body.)

The apparent velocity was calculated from the net acceleration using the cumulative trapezoidal rule, which served as the second input time series. This calculation ignored the fact that the direction of the acceleration vector was unknown because it was based on the resultant. Nevertheless, this pseudo-velocity served its purpose by providing the equivalent metric for the relevant discrete features, originally devised for vertical accelerations [20]. Using the resultant acceleration and the pseudo-resultant velocity, a pseudo-power time series was obtained by taking the instantaneous acceleration and pseudo-velocity at each point in the time series.

2.3. Continuous Feature Extraction

The continuous features were extracted using functional principal component analysis (FPCA), which is based entirely on the variance in the data [27]. Hence, these data-driven features were discovered automatically without applying any domain-specific knowledge. As described below, the procedure involved padding the time series to a standard length, aligning the signals, converting them into smooth functions, and then running FPCA to yield continuous features. The shape of each functional principal component (FPC) effectively defined the continuous feature, corresponding to a particular mode of variation in the resultant acceleration waveform. Their associated FPC scores were the inputs to the models.

First, the time series were padded out to give them all the same length as the longest series in the sample. Points were appended to the end of the series, equal to the last value before padding. No signal filtering was performed because functional smoothing performs the same purpose of penalizing high-frequency oscillations.

The padded time series required alignment so that FPCA would capture amplitude variance between the signals. Based on our previous research, we opted to align the signals by making a linear offset to the time series rather than using curve registration, which has the disadvantage of distorting the waveforms to enforce maximal alignment [28,29]. We developed five alignment algorithms to align the signals based on cross-correlation and landmark identification, two common approaches when applying a linear offset to the signals. Having several candidate methods allowed us to determine the best approach specific to our respective wearable sensor datasets. The cross-correlation methods aligned the signals to a reference signal, which was either the mean signal (*XCMeanConv*) or a randomly chosen signal from the sample (*XCRandom*). The landmark methods identified either a peak immediately before takeoff (*LMTakeoffPeak*), the takeoff instant identified by the discrete feature-extraction algorithm (*LMTakeoffBiomechanical*), or the peak associated with landing (*LMLandingPeak*). For the Accelerometer dataset, we also had the actual takeoff time for reference (*LMTakeoffActual*), as determined from the force plate VGRF data. Further details on our signal alignment methods can be found in Appendix A.2, along with their evaluation in Appendix B.1.

After the time series were padded and aligned, they were converted into continuous, smoothly varying functions with a b-spline basis of fourth order, regularized with a 1st-order roughness penalty. For further details of this automated procedure, refer to Appendix A.3.

Finally, FPCA was performed on the functional representations of the padded and aligned time series to obtain the FPCs that defined each continuous feature's characteristic shape. The associated FPC scores were calculated for each signal by computing the inner product of its functional curve with each respective FPC.

2.4. Feature Selection

We evaluated models based on three feature sets from each dataset: discrete features, continuous features, and a hybrid set that combined both feature types. Our investigation first considered the qualities and efficacy of the discrete and continuous features in isolation before introducing the combined feature set. The combined feature set also included the VMD features from the Mascia et al. [20] study that had been excluded from our prior comparison set owing to their continuous nature. A correlation matrix revealed the relationship within and between discrete and continuous features. We also calculated the Variance Inflation Factor (VIF) to detect multicollinearity in the models, which is usually defined as when $VIF > 10$ [30].

As part of research question 1, we restricted the number of features, forcing the model to choose the most valuable features to predict jump peak power. The chosen feature-selection method was based on Lasso regression using least squares. Lasso is a regularized linear model in which high beta coefficients are penalized. Depending on the regularization parameter, the L1 regularization forces some of those beta coefficients to zero, therefore effectively removing the associated predictors from the model. The feature-selection algorithm fitted 100 models across a wide range of values for the regularization parameter, λ , to find which value yielded the desired number of predictors with non-zero coefficients. If λ values resulted in models with too many predictors or too few but not the number required to meet the specified sample size, the λ range was narrowed, and the procedure was repeated. The selected features were then input directly to all model types, which in the case of Lasso meant re-fitting the model with the pre-determined λ . Thus, the non-zero coefficients from the Lasso feature-selection model were not utilized.

When applied to the combined feature set, feature selection offered a direct comparison between feature types. The extent to which discrete and continuous were favored revealed the relative efficacy of each feature type based on the probability of selection and the mean absolute beta coefficients for selected features. We initially restricted the number of features to five and then eased the restriction to 10 and then 15 to see which other features were progressively included.

2.5. Dataset Truncation

To answer research question 2, we downsized the datasets progressively to evaluate the models' sensitivity to sample size. Participants were added at random, one by one, to the smaller dataset, including all their jumps, until the number of jumps reached the required number for the sample, as specified by the investigation. When adding the last participant to be included, their block of jumps could make the sample larger than it should be. In this case, jumps were removed at random from any participant already included until the dataset was shrunk to the required volume.

2.6. Models

Having extracted discrete and continuous features characterizing the jumps, we used them as separate or combined groups of predictors in a range of regression models to predict peak external power. We chose the following regression models as being representative of the different types of models that may be employed to address similar research questions:

- a linear model allowing for extensive inference of the model fit, including explained variance, shrinkage, and other statistics that can support our investigation;
- Lasso linear regression using L1 regularization to handle potentially large numbers of predictors and curb overfitting [31];
- a support vector machine (SVM), a non-parametric model to serve as an alternative to the linear parametric models above [32]; and
- XGBoost, as a tree ensemble model based on gradient boosting [33], which is highly regarded in the machine-learning community for its versatility as demonstrated by winning many Kaggle competitions [34].

The models were trained to predict peak power based on the three aforementioned feature sets standardized to z-scores prior to fitting. The mean and standard deviations for the training features were also retained as model parameters and used to standardize the validation features to the same scale. The outcome variable, peak power, was also standardized in this way, so the linear model produced standardized beta coefficients. This standardization was applied to all models, allowing for a fair comparison between datasets by removing differences in performance levels between the cohorts as a confounding factor.

The models were subject to Bayesian optimization through MATLAB's automated hyperparameter optimization procedure, except for the linear model, which has no tunable hyperparameters. Two-fold cross-validation (CV) was chosen to maximize validation set size and improve the likelihood of selecting the true best model [35]. As many thousands of model fittings would be performed, the optimization procedure was limited to 20 iterations to keep the computational cost manageable.

2.7. Evaluation

We employed a two-fold CV to evaluate the models, repeated 25 times to make 50 model fits, and provided a representative assessment. The one exception was for the sample size investigation, which involved 10 dataset truncations and 5 two-fold CV repeats, making $10 \times 5 \times 2 = 100$ model fits, double the previous number of fits to address the higher variance observed between fits for small sample sizes. Two-fold CV provides a large validation set that serves to increase the variance in validation error between models, making it ideal for model comparisons, albeit at the expense of inflating the validation error [35].

The datasets were partitioned at the participant level, so a person's jumps only appeared in the training or validation datasets. Each model was evaluated on the training and validation sets using several metrics. The principal measure of model performance was the root mean squared error (RMSE) in predicted standardized peak power. Other metrics relating to evaluation can be found in Appendix A.2.

Model performance was explored over a range of configuration settings using grid searches. The configuration setup encompassed parameters controlling every aspect of their operation, including the feature-extraction methods, feature selection, dataset truncation, and the modeling procedure. All procedures described above, including the statistical analysis, were implemented in MATLAB R2023b (Mathworks Inc., Natick, MA, USA), <https://github.com/markgewhite/jumpsensormodels> (made available from 12 April 2024).

2.8. Full Modeling Procedure

The guiding principle behind applying CV in our study was to obtain an unbiased estimate of the model's performance on unseen data. By performing the entire modeling procedure, including data preprocessing (filtering for discrete features, alignment for continuous features), feature extraction, feature selection, model fitting, and optimization, within each training fold, we ensured that the CV error reflects the error we can typically expect when applying these same methods to new, independent datasets. (The discrete features for a given signal would always have the same values irrespective of the subsample in which it was present.) The cross-validated RMSE provides a realistic assessment of how well the models would generalize to unseen data. Its calculation depends on considering the potential variations in key determinants dependent on the data distribution. Such determinants include reference points or signals used in the alignment methods, the roughness penalty for functional smoothing, the FPC definitions themselves, and the optimized hyperparameters of the fitted models. This robust approach goes beyond simply enabling the cross-validation option for a model function. It ensured no "information leakage" between training and validation sets [36,37]. However, it comes at a greater cost because the same procedures are repeated multiple times with slightly different results each time. Nonetheless, this is essential for our purpose if we are to build models that are generalizable to future applications and answer our research questions.

3. Results

3.1. Continuous Feature-Extraction: Alignment Evaluation

The evaluation of the alignment methods for FPCA concluded that *XCMeanConv* was best for both datasets (Appendix B.1). This convergent cross-correlation method yielded the lowest alignment RMSE, the highest Pearson correlation, and the highest signal-to-noise ratio (SNR) for their respective datasets. It was noted that the choice of alignment method could have a material effect on the shape of the FPCs.

We then extended our alignment evaluation to consider the consequential impact on the models' performance. For the Smartphone dataset, the lowest model validation error was achieved with *LMTakeoffBiomechanical* for all models except *XGBoost*. This finding contrasts with the results based solely on alignment metrics, although in the latter case, the difference was marginal (Figure 2). Moreover, *LMTakeoffBiomechanical* had the worst alignment metrics for the Smartphone dataset (Figure A2). Notably, *XCMeanConv* achieved the lowest training error across all models, indicating that the poor validation error associated with this method was likely due to overfitting.

The Accelerometer dataset was similar in that the best alignment method, *XCMeanConv*, did not yield the lowest model validation error. Instead, *LMTakeoffPeak* from our candidate methods achieved the lowest validation error. However, *LMTakeoffActual*, the true takeoff time only included as a reference, outperformed all model types in this regard. *XCMeanConv* did achieve the lowest training error, indicating that the best alignment method induces overfitting in the models. In general terms, however, the models based on Smartphone data had a greater tendency to overfit, given the wider differences between validation and training error. *XGBoost* had the lowest training errors, yet the validation error was similar to the other models. The SVM models revealed the least overfitting. To conclude, the alignment method that was the best model validation performance did not produce the most closely aligned curves.

For the following analysis, we chose *LMTakeoffPeak* alignment for both datasets based on its consequent low model validation errors. It produced the lowest validation RMSE across all Accelerometer models and only a slightly higher validation RMSE than *LMTakeoffBiomechanical* for the Smartphone models, especially given the large RMSE variance between model fits. Having the same alignment method for both datasets was also considered advantageous as it made them more comparable.

3.2. Feature Characteristics

There was no correlation between the continuous features, which are orthogonal by definition, but there was a high degree of correlation between the discrete features (Figure 3). Moreover, from the extended correlation matrices that include both sets of features, it is evident that there were only weak correlations between the discrete and continuous features, indicating that they are largely distinct from one another. The strongest correlations with the discrete features were found with FPC1-3.

The continuous features were generally normally distributed, but many of the discrete features were not (Appendix B.2). Several discrete features exhibited long tails and moderate skew.

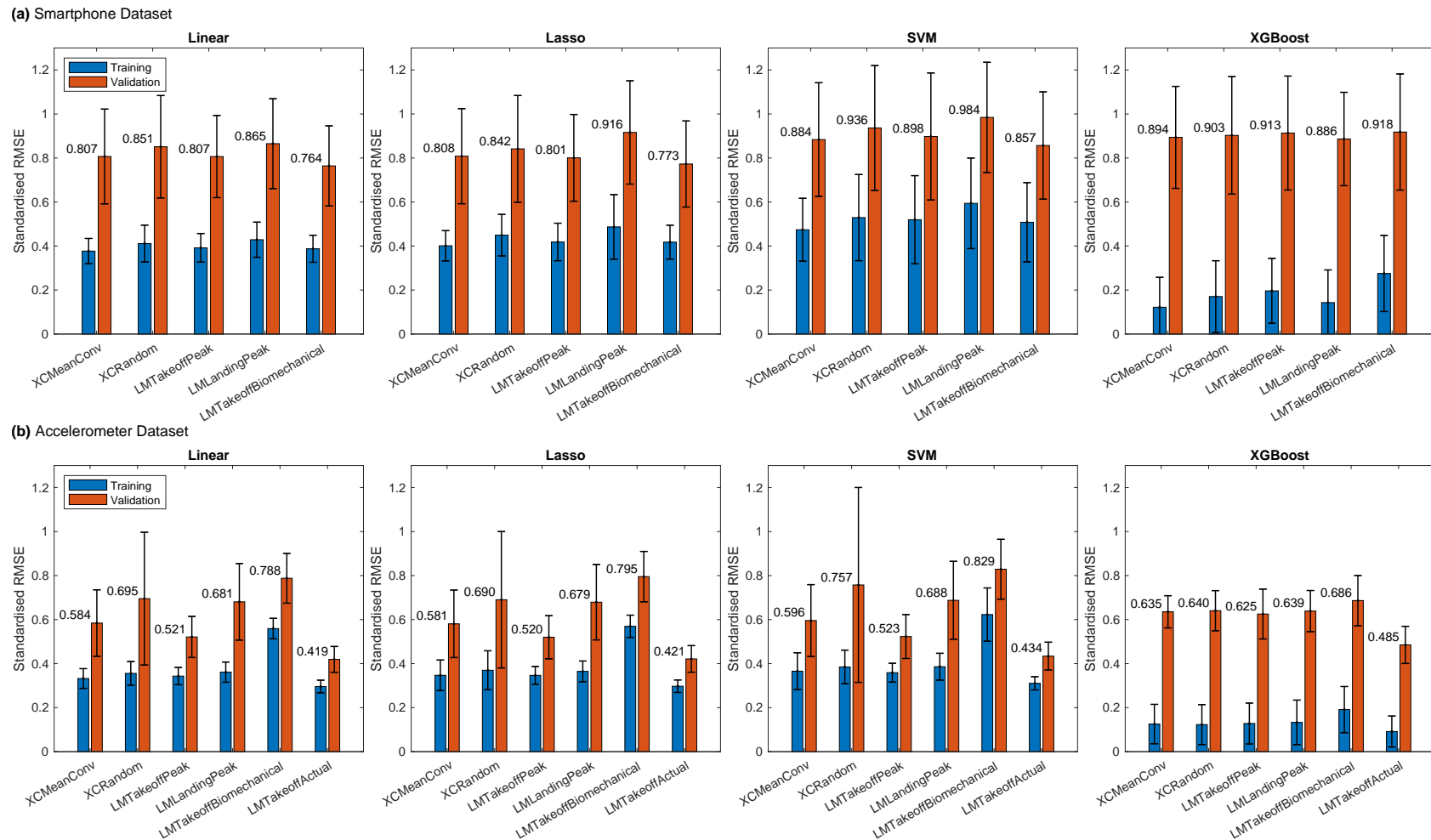


Figure 2. Model performance using continuous features for different alignment methods. Standardized RMSE is in z-scores for jump peak power. Model performance is averaged over 50 model fits (25×2 -fold CV) from the same run as for Figure A2. The mean validation error is shown next to each red bar. The error bars show the standard deviation between model fits.

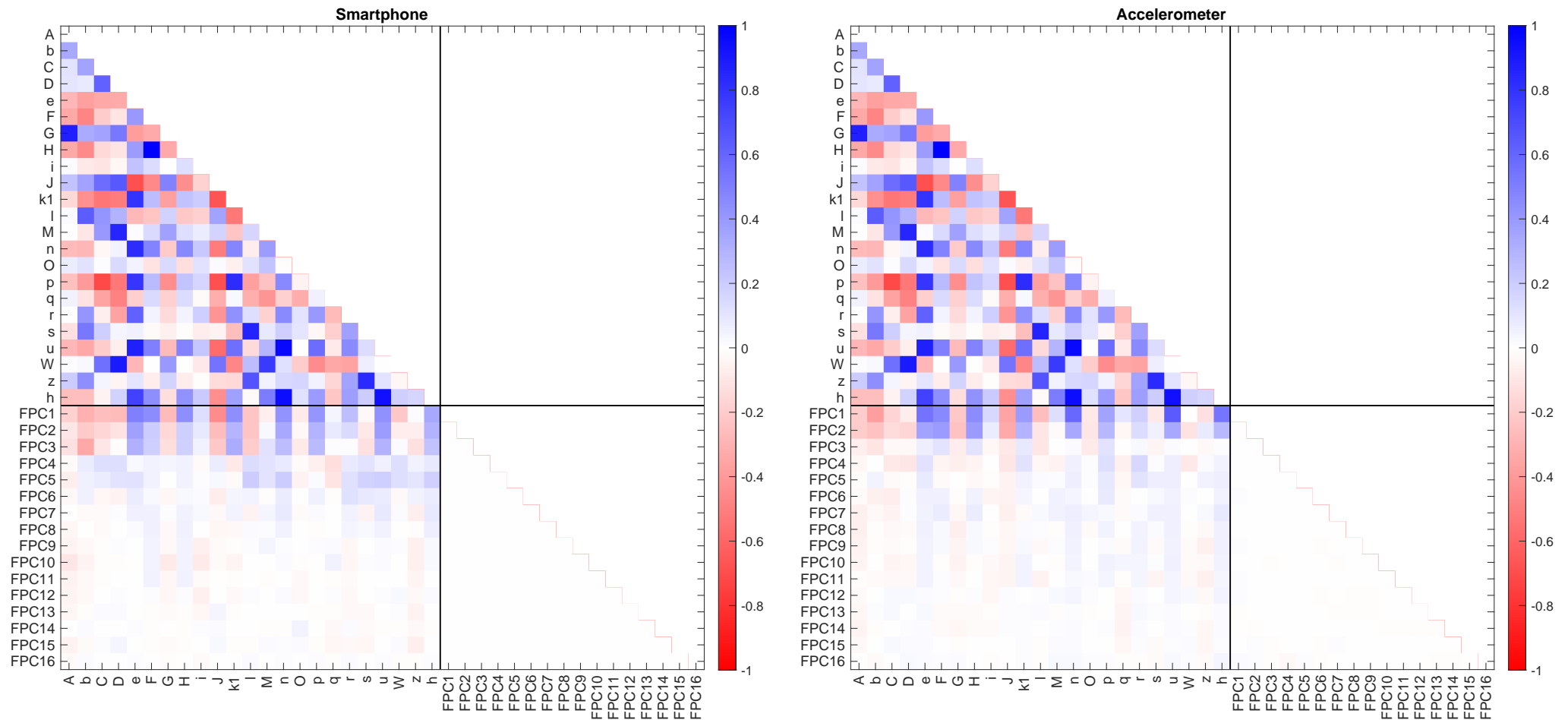


Figure 3. Correlation heatmap within and between feature-extraction methods for Smartphone and Accelerometer datasets averaged over 50 training folds (25×2 -fold CV). Note the high correlations within discrete features (top-left quadrant), whereas the correlations between discrete and continuous features are comparatively weak except for those with FPC1 and FPC2 (lower left quadrant). There are no correlations within continuous features, FPC n (black lower right quadrant).

3.3. Linear Model Inference

We examined several statistics from linear models fitted to each dataset to gain further insight into the qualities of the discrete and continuous features (Table 2). These statistics helped us compare the performance and characteristics of the models when using either discrete or continuous features. The linear models fitted with continuous features showed better performance for both datasets, as demonstrated by lower training errors, higher F-statistics, and greater variance explained. Additionally, the continuous feature models exhibited lower shrinkage, indicating less overfitting. The discrete feature models had a lower proportion of outliers compared to the continuous feature models. However, the outlier proportions for both the Smartphone and Accelerometer datasets (0.042 and 0.014, respectively) were below 0.05, suggesting a narrow, peaked distribution that deviated from normality. This deviation from normality could potentially affect the validity of the linear model’s assumptions and its sensitivity to outliers, although the impact may be limited given the relatively small deviation and the sample size.

It is also important to note that discrete features had an extremely high level of multicollinearity. Three predictors had $VIF > 100$, and for a further seven, VIF was infinite. In other words, those features could be explained perfectly by a suitable linear combination of other variables. This multicollinearity brought considerable uncertainty to the contribution of individual features, as detailed in Appendix B.3).

Table 2. Comparison of encoding methods for each training dataset based on the linear model’s statistics and associated metrics. Mean and SD compiled from 50 model fits (25×2 -fold CV). Emboldened values for each dataset indicate superior performance. Note that this is training, not validation performance.

Dataset	Encoding	Standardized Training RMSE *	F-Statistic †	Explained Variance, R ²	Shrinkage ‡	Proportion Outliers ^a	Proportion Highly Correlated ^b
Smartphone	Discrete	0.430 ± 0.062	8.34 ± 3.04	0.808 ± 0.055	0.108 ± 0.033	0.042 ± 0.018	0.827 ± 0.032
	Continuous	0.392 ± 0.065	15.8 ± 6.3	0.840 ± 0.053	0.061 ± 0.021	0.054 ± 0.018	0.000 ± 0.000
Accelerometer	Discrete	0.469 ± 0.041	24.3 ± 5.9	0.777 ± 0.039	0.034 ± 0.007	0.014 ± 0.015	0.831 ± 0.059
	Continuous	0.343 ± 0.039	75.8 ± 18.3	0.880 ± 0.029	0.012 ± 0.003	0.052 ± 0.012	0.000 ± 0.000

* Standardized as z-scores for comparison between datasets. † Ratio of the model’s explained variance (all predictors) to that of the null model (intercept only), i.e., how well the model explains the data. ‡ Estimated reduction in explained variance if the model is applied to new data from the same population. ^a Proportion of observations considered outliers, as defined by Cook’s distance exceeding $4 \times$ training set’s mean distance. ^b Proportion of predictors with high multicollinearity, as defined by the Variance Inflation Factor, $VIF > 10$.

3.4. Model Performance

The performance of the model types was assessed as a function of the number of predictors using discrete, continuous, or combined feature sets with the latter including VMD features (Figure 4a). The training error was lower for models using continuous features than discrete features. The combined feature set sustained the downward trend in training error as more features were added to the models. In the case of the SVM, Lasso, and XGBoost models using either discrete or continuous features from the Smartphone dataset, the training error initially fell and then rose as the number of features increased. In the case of the Accelerometer dataset, the training error tended to fall asymptotically as the number of features increased. In all cases, the XGBoost model consistently yielded the lowest training error. The uncertainty (interquartile range indicated by error bars) for the Accelerometer training errors was smaller than that of the Smartphone dataset. In some cases, the error bars were so large that there was considerable uncertainty in the trend lines obtained using a Gaussian process best fit.

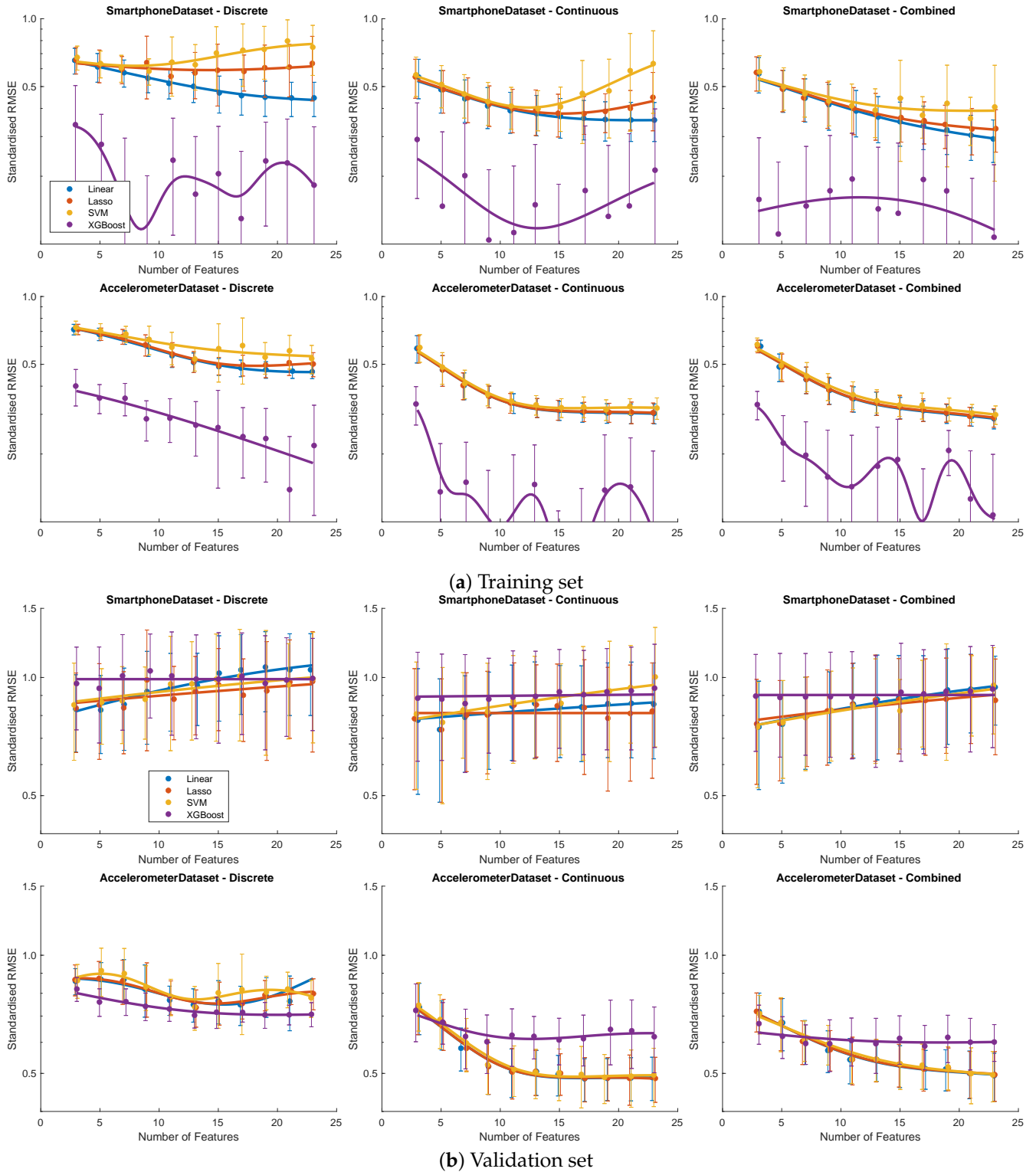


Figure 4. Performance of the four model types as a function of the number of features selected. Standardized RMSE (log scale) is the median of 50 model fits (25×2 -fold CV), where the error bars represent the interquartile range. A standardized error > 1 indicates performance worse than the null model, defined as a constant equal to the mean peak power. Best fit lines based on Gaussian regression using a Matern 5/2 kernel.

The validation errors were higher than the training errors, more so for the Smartphone models than the Accelerometer models (Figure 4b). The linear, Lasso, and SVM models all tended towards higher validation errors for the Smartphone dataset as the number of features increased, but this trend was uncertain. Only the XGBoost model seemed unaffected by this apparent overfitting, given a flat trend. It was only with the Accelerometer data that there was a clear reduction in validation error as the number of features increased, most clearly when using continuous features or the combined features set when using the linear, Lasso, and SVM models, which all produced similar error levels. For the Accelerometer dataset, the XGBoost validation errors were lower when using discrete data, but it did not respond as the other models did when using continuous data.

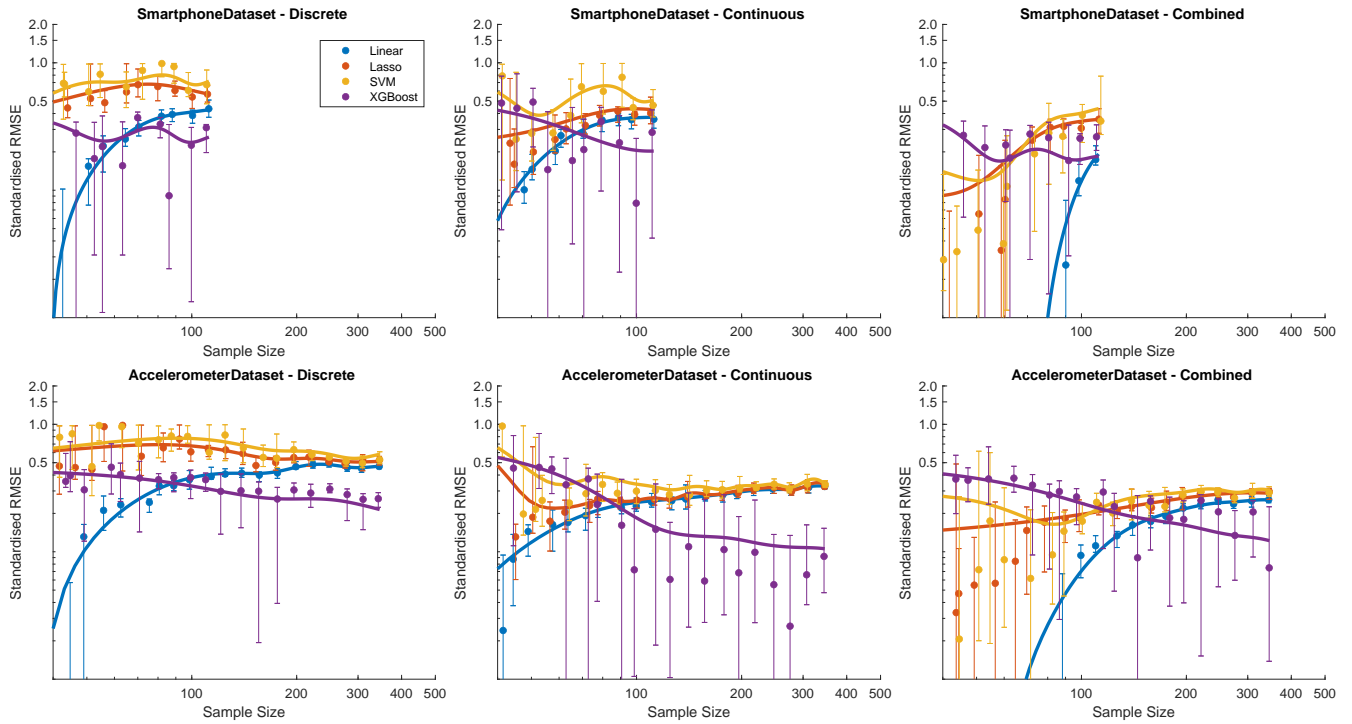
3.5. Sample Size Truncation

The model robustness and sensitivity to data volume (research question 2) were reflected in changes in model performance when the datasets were capped at an increasing number of observations (Figure 5a). The training error generally rose and then plateaued as the available data were enlarged for both datasets and all three feature options. One specific exception was where it fell slightly when the Lasso and SVM models used discrete Accelerometer features, while XGBoost models continued to improve their training errors as the sample size increased. The training error initially declined for the Lasso and SVM models when continuous features from the Accelerometer dataset were used. As mentioned above, the large variation in error between model fits made trends harder to discern.

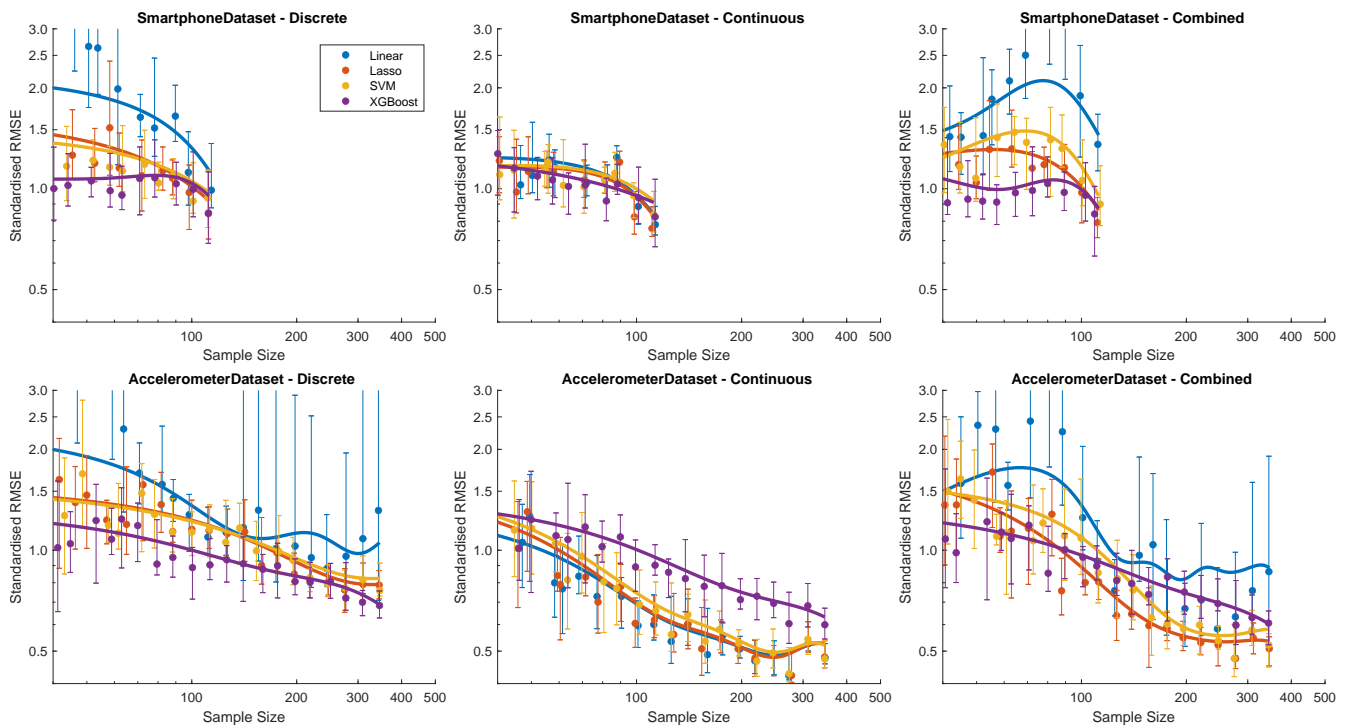
As with training, the validation error was lower for XGBoost except with continuous Accelerometer features, although the gap to other models narrowed at higher data volumes (Figure 5b). Again, Lasso, SVM, and linear models produced the best validation estimates for the Accelerometer datasets. Linear models trained on discrete features produced large validation errors, which could vary substantially between model fits, especially with small samples.

3.6. Feature-Selection Preference

Restricting predictor numbers from the combined feature set revealed the relative efficacy of discrete and continuous features (research question 1), as highlighted by the feature-selection process (Figure 6). The plots showing the probability of selection revealed a strong preference for the continuous features across both datasets (research question 3). The models often favored FPC1, and as the restriction on the number of predictors was gradually lifted, many of the FPCs were present in around half of the models. The VMD features, which were included at this stage of the analysis, were rarely chosen. The discrete features were more prominent when few predictors were required. u and $k1$ (mean concentric power and acceleration at the end of the braking phase, respectively) were often present. The mean absolute value of the beta coefficients when these discrete features were present demonstrated that the FPCs were the dominant factors in the model. The discrete features' influence on the outcome variable was relatively minor.

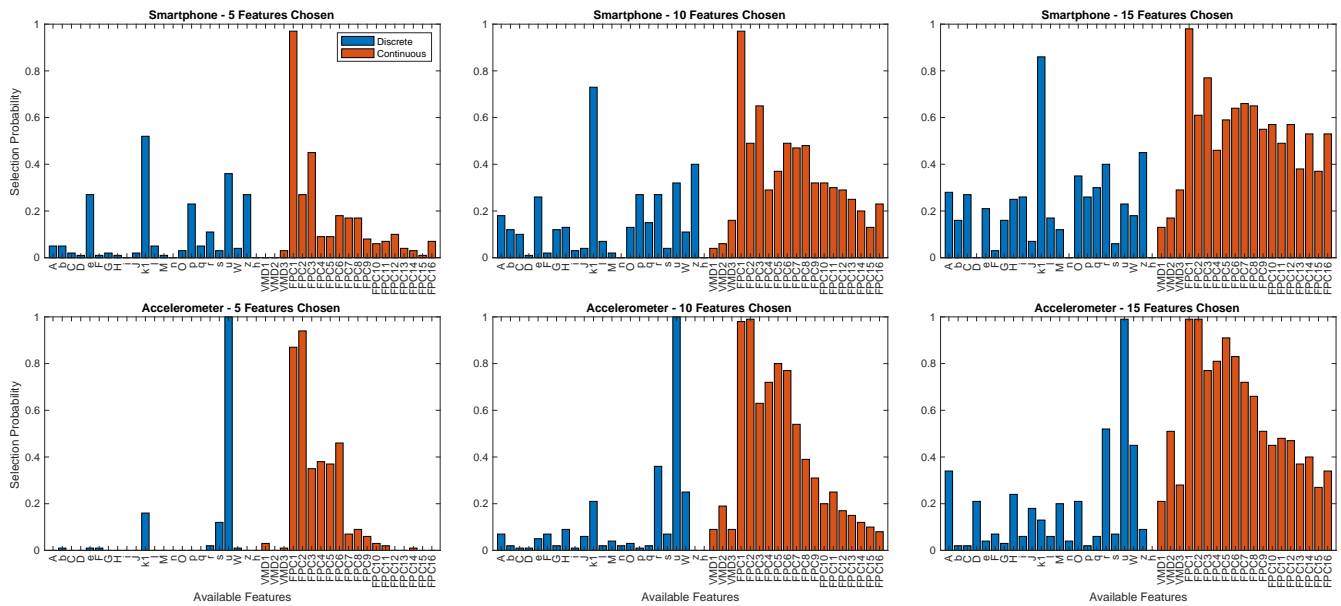


(a) Training set

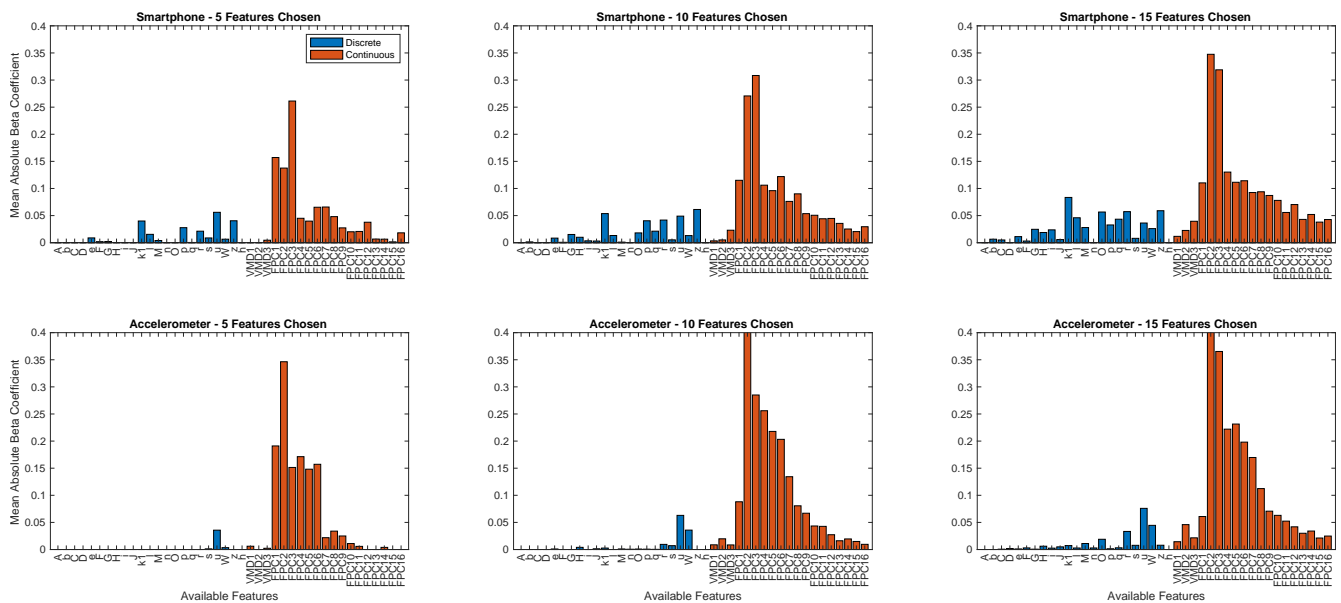


(b) Validation set

Figure 5. Model performance as a function of sample size when the number of observations is capped. Standardized RMSE is the median over ten random subsets, each involving 10×2 -fold CV, making up 200 model fits for each point. The error bars represent the interquartile range. Best fit lines based on Gaussian process regression using a Matern 5/2 kernel.



(a) Selection Probabilities



(b) Mean Absolute Beta Coefficients

Figure 6. Predictor selection for the combined feature set when restricting the models to 5, 10, or 15 features. (a) Probability of a feature being selected over 50 training samples (25×2 -fold CV). (b) Mean absolute beta coefficients from when those features were selected. Please note that the continuous predictors include VMD and FPC features.

4. Discussion

This study investigated the efficacy of discrete and continuous feature-extraction methods, separately and in combination, for modeling athletic performance using wearable sensor data. By comparing these approaches across two datasets with different sensor types and placements, as well as with a variety of different models, we aimed to provide insights into the robustness and generalizability of these methods. Our findings demonstrate the superiority of continuous features, particularly those derived from FPCA, in terms of model performance, robustness to variations in data distribution and volume, and consistency across different datasets. Specifically, we found that (1) continuous features, especially FPCs, consistently outperformed discrete features in modeling CMJ peak power output; (2) models based on

continuous features were more robust to variations in data distribution and volume compared to discrete feature models; and (3) the consistency of our results across datasets differing in sensor type and placement supports the generalizability of our findings.

4.1. Research Question 1: Feature-Extraction Efficacy

Our investigation revealed that continuous features, specifically FPCs, outperformed discrete features in modeling peak power output during countermovement jumps (Figure 5b). These findings are based on a rigorous and comprehensive modeling approach encompassing the entire process, from data preprocessing to model evaluation. By applying this full modeling procedure within each cross-validation fold, our results provide a robust and realistic assessment of model performance on unseen data, avoiding potential biases arising from information leakage. The independence of FPCs, as demonstrated by the correlation matrix analysis, contributed to their robustness and ability to capture valuable temporal information. In contrast, discrete features exhibited high multicollinearity, leading to less reliable models and overfitting. These findings support the approach taken in previous research that used continuous features to distinguish between groups based on characteristic patterns in the data [12,13,38]. The evidence from the correlation matrix (Figure 3) suggests that the notion that FPCs may sometimes be largely equivalent to discrete features of peaks and troughs is incorrect. FPCs take the whole waveform into account, and the influence of curves away from the peak in question serves to regularize the components, providing an advantage for the models based on these features.

The discrete features' beta coefficients varied greatly between the training subsamples (Figure A5), particularly in the Smartphone models, indicating considerable uncertainty in their true values. This uncertainty made it difficult to conclude which discrete features contribute strongly to performance outcomes. It, therefore, limits the practical value of discrete features, contrary to their apparent intuitive interpretability, which has often been seen in the biomechanics field as their chief advantage over other types of features. In contrast, the beta coefficients for the continuous features exhibited lower variance and more consistent values across subsamples, suggesting that FPCs provide a more reliable basis for modeling athletic performance. However, it is important to note that wearable sensor signals are inherently noisy and more challenging to interpret than traditional measures such as ground reaction forces. As a result, the choice of sensors and feature-extraction methods should prioritize practical considerations and model performance over interpretability alone.

4.2. Research Question 2: Model Robustness

Our results showed that continuous feature models, particularly those using FPCs, were more robust to variations in data distribution and volume compared to discrete feature models (Figure 5). Continuous feature models were able to make effective use of additional predictors, lowering validation error only when applied to the Accelerometer dataset. In contrast, for the Smartphone dataset, the validation error tended to rise with more features included. This difference in performance may be attributed to the Smartphone's looser coupling with the body's center of mass—the handheld device allows for greater extraneous motion compared to that of the Accelerometer, which is taped firmly to the skin. The Accelerometer would still move due to skin movement artifact, but it would do so in a more predictable fashion compared to the Smartphone. In comparison, the discrete feature models suffered from increasing levels of overfitting and worsening validation errors (Figure 4). These results highlight the need for feature selection to limit the number of features of either type. However, Lasso regularization can alleviate, to some extent, the issue of multicollinearity.

An unexpected observation from our sample size truncation analysis was the initial increase in training error for most models as the dataset size increased, followed by a plateauing trend (Figure 5). This phenomenon suggests that smaller datasets may not capture the true complexity of the underlying relationships, leading to an underestimation

of the training error. Interestingly, XGBoost was less susceptible to this effect, as its training error consistently decreased with increasing sample size. This robustness could be attributed to XGBoost's ability to effectively capture complex non-linear relationships and its inherent regularization techniques, which help prevent overfitting [33,34].

The choice of the best-performing model may depend on the specific circumstances and dataset characteristics, confirming the well-known importance of evaluating a range of models for each application. Linear models, despite their simplicity, can provide valuable insights into the relationships between features and performance outcomes, as demonstrated by the analysis of beta coefficients in our study (Figure A5). Lasso is also a linear regression model whose beta coefficients can also be interpreted similarly, but it has the added advantage of handling multicollinearity, making it a reasonable choice when working with discrete features. However, it was XGBoost that tended to yield lower validation errors than the other models when using discrete features in smaller samples or when more features were included, demonstrating its robustness for limited datasets or where domain expertise suggests there are potentially a large number of features that may be relevant. When using continuous features exclusively, XGBoost was outperformed by Lasso and SVM, and even the linear model provided sufficient FPCs and observations. In summary, these findings underscore the need for careful consideration of model robustness and sample size when selecting feature-extraction methods and developing athletic performance models.

4.3. Research Question 3: Generalizability

The consistency of our results across the Accelerometer and Smartphone datasets demonstrates that our findings—the superior performance of models using continuous features and their greater robustness to variations in data distribution and volume—are generalizable across different data-collection protocols. However, the differences in corresponding FPC waveforms between datasets and the under-performance of Smartphone models compared to Accelerometer models suggest that sensor characteristics, location, and attachments can impact model performance.

Specifically, the Smartphone models exhibited higher validation errors (Figure 4b) and a greater tendency to overfit as the number of features increased (Figure 5b), which may be attributed to the handheld Smartphone's looser coupling to the body's center of mass. Moreover, the Smartphone models consistently yielded higher training errors than the Accelerometer models (Figure 4a), indicating that the Smartphone data may be more challenging to fit, even with a larger number of features. These performance disparities persist even when considering the difference in sample sizes between the datasets, as the Smartphone models still underperform relative to the Accelerometer models at equivalent sample sizes (Figure 5).

These findings underscore the importance of considering not only data-collection protocols but also the inherent limitations of sensor placement and attachment when developing athletic performance models [2]. Notwithstanding this difference, our main findings were generally consistent across the datasets, reinforcing the superiority of continuous features and the challenges associated with discrete features, thus bolstering the generality of our conclusions.

4.4. Acceleration Signal Type

In this study, we focused on using the resultant acceleration for direct comparability between the Smartphone and Accelerometer datasets, even though the Smartphone data included gyroscope measurements that could have been used to compute the vertical acceleration component. While the vertical component is more pertinent when estimating jump performance, given that the peak power (ground truth) was calculated using the vertical ground reaction force, our preliminary research revealed that models based on the resultant acceleration yielded lower validation errors than those using the vertical acceleration. This unexpected finding suggests that the machine learning approach, which relies on patterns

in the data, can effectively handle the resultant acceleration by implicitly adjusting the model parameters to account for the motion in other principal axes. Furthermore, using the resultant acceleration may have a regularizing effect, reducing the risk of overfitting compared to using the vertical component alone. These results challenge conventional thinking in biomechanics and highlight the need for future research to investigate alternative signal representations and their impact on model performance, given the additional information from other signals that may enhance predictive accuracy. The optimal choice of input signal may not always align with traditional assumptions.

4.5. Alignment Methods

This study employed relatively simple alignment methods, such as cross-correlation and landmark-based methods, compared to more sophisticated approaches like curve registration (dynamic time warping) or linear time transformations. Interestingly, we found that the model validation performance was better when using signals that were not optimally aligned (e.g., *LMTakeoffPeak*) according to our metrics. This key finding emphasizes the trade-off between alignment and preserving valuable phase information captured by FPCs, as was evident in the phase-shift properties observed in some FPCs (Figure A3). The temporal position of peaks in component plots shifted as the FPC score varied, an effect more apparent in FPC1 and FPC3 with *LMTakeoffPeak* alignment.

Our findings, along with previous research [28,29,39], suggest that enforcing a higher degree of alignment through curve registration or linear time transformations may be detrimental to the performance of models similar to those in our study. These sophisticated alignment methods often result in distorted waveforms, hindering the model's ability to capture relevant phase information, even when phase information from the time domain transform is included in the model [28]. In a previous study using the same Accelerometer dataset, we found that landmark registration was detrimental to the peak power model compared to the non-registered condition and that models depended on the variance in flight time ([29], Sections 6.4.4–6.4.5).

The choice of alignment method can also materially affect the shape and interpretation of the FPCs, determining which aspects of the jump are emphasized in the components. For example, in the Accelerometer dataset, FPC1 captured the variation in acceleration during the braking phase when using *XCMeanConv* alignment but captured the variation in flight duration primarily when using *LMTakeoffPeak* alignment. These differences in FPC characteristics underscore the importance of carefully selecting an alignment method that preserves the relevant phase information and enhances the interpretability of the components, ultimately contributing to a clearer understanding of the aspects of the jump that influence performance.

4.6. Limitations and Future Directions

First, our analysis was based solely on the resultant acceleration to ensure comparability between the datasets. There are other ways to represent acceleration, but although we found that the vertical acceleration component was less effective, there are other representations, such as using all three signal dimensions. Exploring these alternative signal representations could lead to more accurate and informative models. For instance, using the vertical acceleration component or considering all three dimensions might better capture the key aspects of the jump that contribute to peak power. Furthermore, investigating the optimal signal representation for different sensor types and placements could inform future data-collection protocols, ensuring that the most relevant and informative data are captured for modeling athletic performance.

In our study, we observed that models based on the Smartphone dataset generally underperformed compared to those based on the Accelerometer dataset, possibly due to extraneous motion from the handheld Smartphone degrading data quality. We suggest future research investigate the relationship between data quality and model performance in the context of wearable sensor data for athletic performance assessment. This could

involve quantifying data quality using metrics such as signal-to-noise ratio, outlier detection, or spectral analysis to identify extraneous motion or artifacts. Future research could also explore non-parametric approaches to estimating functional principal components, such as robust FPCA methods, to address potential deviations from normality in the continuous features, particularly for the first few FPCs. While the potential impact of using non-parametric approaches on the overall results may vary depending on the specific dataset and the influence of the first few FPCs, exploring these methods could lead to more accurate representations of the underlying functional data, particularly when significant deviations from Gaussian distributions are present.

Second, our feature-selection procedure relied on Lasso regularization, which has gained popularity owing to its simplicity and effectiveness [40]. It requires only adjusting the regularization parameter to vary the number of features admitted to the model. Other methods may be considered, such as stepwise regression, but it is slower and requires tuning several hyperparameters [40]. Although different selection methods may choose other features, our conclusions are unlikely to be significantly affected, as all selection methods depend on the intrinsic information held by the predictors. The differences in selected features between methods may only be subtle, as the underlying relationships between the predictors and the target variable remain the same. Ultimately, the effectiveness of any feature-selection method is limited by the information available in the dataset.

Thirdly, we inferred feature influence using the standardized beta coefficients in the linear model. While this approach is convenient and provides a direct measure of influence in the linear model, there are other predictor contribution methods available, such as SHAP (SHapley Additive exPlanations) values [41] and LIME (Local Interpretable Model-agnostic Explanations) [42]. These techniques can be applied to various model types and offer a more comprehensive understanding of the features' importance. However, these methods may not always provide a reliable estimate of the predictor's true influence. For example, SHAP values can be sensitive to multicollinearity, while LIME explanations may be affected by the choice of perturbation strategy and the complexity of the local approximation [43,44].

Future research should explore alternative signal representations, investigate the impact of different feature-selection methods, and employ a range of predictor contribution techniques to gain a more comprehensive understanding of feature influence. By doing so, athletic performance models based on wearable sensor data may continue to improve in accuracy, interpretability, and generalizability, and so become more useful to the applied practitioner.

4.7. Practical Implications

Our study has important practical implications for feature extraction and model development in biomechanics. The superiority of continuous features, particularly FPCs, for modeling athletic performance metrics emphasizes the importance of understanding the efficacy of different feature-extraction methods. Our findings suggest that continuous feature extraction can streamline the feature-selection process and reduce the reliance on arduous and time-consuming hand-crafted features [9]. This research has the potential to accelerate the development of accurate and reliable athletic performance models, enabling researchers and practitioners to make more informed decisions about training and performance optimization. While domain knowledge can provide valuable insights, it is crucial to consider the potential biases or false assumptions that may be introduced. Striking a balance between data-driven approaches and domain expertise is essential, ensuring that the models remain objective and evidence-based while still benefiting from domain experts' contextual understanding.

5. Conclusions

Our study advances the understanding of discrete and continuous feature-extraction methods for modeling athletic performance using wearable sensor data. We have shown that continuous features, particularly those derived from Functional Principal Component Analysis, outperform discrete features in terms of model performance, robustness

to variations in data distribution and volume, and consistency across different datasets. By demonstrating the efficacy of continuous features and highlighting the challenges associated with discrete features, we have provided valuable insights for researchers and practitioners in the biomechanics field. Our findings emphasize the importance of considering model robustness, sensor type, and placement, as well as the trade-offs between alignment and preserving valuable phase information when developing athletic performance models. Future research should explore the impact of sensor type and placement on model performance, investigate alternative signal representations, and consider the balance between data-driven approaches and domain knowledge in feature selection.

Author Contributions: Conceptualization, M.W., B.D.L., N.B. and V.C.; methodology, M.W. and B.D.L.; software, M.W. and B.D.L.; validation, M.W., B.D.L., N.B. and V.C.; formal analysis, M.W.; investigation, M.W., B.D.L. and V.C.; resources, V.C. and N.B.; data curation, M.W. and B.D.L.; writing—original draft preparation, M.W.; writing—review and editing, M.W., B.D.L., N.B. and V.C.; visualization, M.W.; supervision, N.B. and V.C.; project administration, N.B. and V.C.; funding acquisition, V.C. All authors have read and agreed to the published version of the manuscript.

Funding: This research was partly funded by Regione Lazio, Call: POR FESR Lazio 2014–2020 ((Azione 1.2.1), grant number 20028AP000000095). The APC was waived.

Institutional Review Board Statement: The study was conducted in accordance with the Declaration of Helsinki. The Smartphone data collection was approved by the Internal Review Board of the University of Rome “Foro Italico”, piazza Lauro de Bosis 6, 00135, Rome, Italy (protocol code No. CAR-94/2021/Rev2022, date of approval: 4 May 2022). The Accelerometer data collection was approved by the Research Ethics and Governance Committee of Swansea University’s College of Engineering (protocol code No. 2018-061, date of approval: 29 May 2018).

Informed Consent Statement: Informed consent was obtained from all subjects involved in the study.

Data Availability Statement: The datasets used in this study were made available on Zenodo at <https://doi.org/10.5281/zenodo.10975077> from 15 April 2024. The MATLAB source code at GitHub <https://github.com/markgwhite/jumpsensormodels>, was made available from 12 April 2024.

Conflicts of Interest: Author Beatrice De Lazzari’s PhD, which encompasses this research, was partly funded by the GoSport s.r.l. The remaining authors declare that the research was conducted in the absence of any commercial or financial relationships that could be construed as a potential conflict of interest. The GoSport s.r.l. had no role in the design of the study; in the collection, analyses, or interpretation of data; in the writing of the manuscript, or in the decision to publish the results.

Abbreviations

The following abbreviations are used in this manuscript:

CMJ	Countermovement Jump
CV	Cross-validation
FPC	Functional Principal Component
FPCA	Functional Principal Component Analysis
GCV	Generalized Cross-Validation
IMU	Inertial Measurement Unit
Lasso	Least Absolute Shrinkage and Selection Operator
LIME	Local Interpretable Model-agnostic Explanations
ML	Machine Learning
RMSE	Root Mean Squared Error
SD	Standard Deviation
SHAP	SHapley Additive exPlanations
SNR	Signal-to-Noise Ratio
SVM	Support Vector Machine
VGRF	Vertical Ground Reaction Force
VIF	Variance Inflation Factor
VMD	Variational Mode Decomposition
XGBoost	eXtreme Gradient Boosting

Appendix A. Methods

Appendix A.1. Discrete Features

Table A1. Discrete feature definitions [20].

ID	Feature	Units	Description
A	Unweighting phase duration	s	$[t_0, t_1]$
b	Minimum acceleration	m/s ²	$a(t_{min})$
C	Time from minimum to maximum acceleration	s	$[t_{min}, t_{amax}]$
D	Main positive impulse time	s	Time duration of positive acceleration from t_{1a} to the last positive sample prior t_{TO}
e	Maximum acceleration	m/s ²	$a(t_{amax})$
F	Time from acceleration positive peak to takeoff	s	$[t_{amax}, t_{TO}]$
G	Ground contact duration	s	$[t_0, t_{TO}]$
H	Time from minimum acceleration to the end of braking phase	s	$[t_{amin}, t_{BP}]$
I	Maximum positive slope of acceleration	m/s ³	$\max(da(t)/dt), t \in [t_{amin}, t_{amax}]$
k1	Acceleration at the end of the braking phase	m/s ²	$a(t_{BP})$
J	Time from negative peak velocity to the end of braking phase	s	$[t_{vmin}, t_{BP}]$
l	Negative peak power	W/kg	$P(t_{pmin})$
M	Positive power duration	s	Self-explanatory
n	Positive peak power	W/kg	$P(t_{pmax})$
O	Time distance between positive peak power and takeoff	s	$[t_{pmax}, t_{TO}]$
p	Mean slope between acceleration peaks	au	$p = (e - b)/C$
q	Shape factor	au	Ratio between the area under the curve from t_{1a} to the last positive sample prior t_{TO} (lasting D) and the one of a rectangle of sides D and e
r	Impulse ratio	au	$r = b/e$
s	Minimum negative velocity	m/s	$v(t_{vmin})$
u	Mean concentric power	W/kg	Average value of $P(t), t \in [t_{BP}, t_{TO}]$
W	Power peaks delta time	s	$[t_{pmin}, t_{pmax}]$
z	Mean eccentric power	W/kg	Average value of $P(t), t \in [t_1, t_{BP}]$
f_1	High central frequency	Hz	Highest VMD central frequency, associated with wobbling tissues and noise
f_2	Middle central frequency	Hz	Middle VMD central frequency, associated with wobbling tissues
f_3	Low central frequency	Hz	Lowest VMD central frequency, associated with the jump proper
h	Jump height	m	Height computed via TOV from a^*

Capital letters are for timings. au = arbitrary units; t_0 = jump onset time; t_{1a} = unbraking–braking phase transition time; t_{BP} = braking-propulsion phase transition time; t_{TO} = takeoff time; t_{amin} = minimum acceleration time; t_{amax} = maximum acceleration time; t_{vmin} = minimum velocity time; t_{pmin} = minimum power time; t_{pmax} = maximum power time.

Appendix A.2. Signal Alignment

Cross-correlation slides one signal over another to find the offset between them where the correlation between overlapping signals is highest. A collection of signals can be aligned by computing the offsets obtained from running cross-correlations between each signal and a common reference signal. The mean signal was chosen as the reference signal for our first candidate method, XCMeanConv. When the signals were out of phase before starting the procedure, the mean signal was a poor reference for aligning the signals. Despite this, the procedure shifted signals into closer alignment with each other. A revised mean signal could then be recalculated, which would become a better representation of the general pattern. Repeating the alignment procedure with the revised mean signal improved the overall alignment further. With further iterations, the mean signal converged to what may be considered the archetypal signal for the sample. Convergence was reached when the change to the mean signal variance over successive iterations fell below a tolerance of 0.001. Typically, 8–9 iterations were required. Our second candidate method, XCRandom, used a randomly chosen signal from the sample to serve as the reference signal so that this

approach served as a comparator to `XCMeanConv`. The signals were aligned once to that randomly chosen reference signal with no further iterations.

Three candidate methods used landmarks to align the signals. The signals were phase-shifted in these methods, so the chosen landmark coincided with a reference position. The choice of reference position is essentially arbitrary so long as its position does not cause the shifted signal to be truncated. We defined the reference position as the average landmark position across the sample. We chose landmarks associated with takeoff and landing as appropriate events that can be readily identified. The alignment objective is to identify a landmark that allows FPCA to capture the relevant amplitude variance and maximize model performance. Therefore, an effective landmark is not necessarily one that accurately identifies the timing of the biomechanical event precisely (takeoff or landing), although that may be the case. It could be that a landmark identified with a peak associated with takeoff and landing may be more effective because it is more in keeping with FPCA's focus on amplitude variance.

We defined two candidate landmark methods based on the two most prominent peaks in the acceleration, approximating takeoff and landing. We smoothed the signal first using a moving average with a 0.5 s window so the peak position was more representative of the general rise in acceleration and not biased by noise. `LMTakeoffPeak` was the first of those peaks in time and `LMLandingPeak` was the second. Prominence was one of the metrics returned by the MATLAB `findpeaks()` function. Our third candidate method, `LMTakeoffBiomechanical`, attempts to locate the takeoff time as a discrete feature accurately. Specifically, the landmark was the instant when the sensor's inertial acceleration first dropped below the acceleration due to gravity (i.e., when $a(t) < -g$) once the computed velocity had risen above zero after passing through its first minimum. Finally, `LMTakeoffActual` was implemented to compare with the true takeoff time or ground truth. It gave the takeoff point from force plate data when VGRF first fell below 10 N and was considered. This information was only available for the Accelerometer dataset.

The quality of signal alignment was evaluated based on comparisons between signal pairs, averaged across all possible pair comparisons, and further averaged across 50 model fits (25×2 -fold CV). The signal-pair comparison metrics were Alignment RMSE (the difference in magnitude between pairs of signals, standardized to z-scores, averaged across their entire length); Pearson Correlation (as the linear correlation between signal pairs); and the Signal-to-Noise Ratio (SNR, the ratio signal power to noise power, defined here as the squared difference between the signal pair: $(a_1 - a_2)^2$).

Appendix A.3. Functional Smoothing

The time series were converted into continuous, smoothly varying functions with a b-spline basis of fourth order [27]. The number of basis functions was scaled with the duration of the time series at a rate of one basis function for every 0.04 s (5.12 points for Smartphone data, 10 points for Accelerometer data). By definition, the fourth-order basis functions have three quarters overlap with their immediate neighbors, giving greater flexibility to follow the time series than may be expected from the function density alone. We found that this relatively low function density yielded lower model validation errors and was quick to execute. FPCA cost rises exponentially as more basis functions are added.

The basis functions were regularized using a 1st-order roughness penalty, with the roughness parameter, λ , determined by an automated generalized cross-validation (GCV) procedure. We used MATLAB's `fminbnd()`, a simple local optimizer, to find λ that minimized GCV error, where $\log_{10} \lambda \in [-10, 2]$. We found that penalizing high rates of change in the signal's curvature (1st order) produced lower GCV errors than the more conventional approach of penalizing high curvature (2nd order). This finding may be attributable to the high rates of change in acceleration on landing.

Appendix B. Extended Results

Appendix B.1. Alignment Evaluation

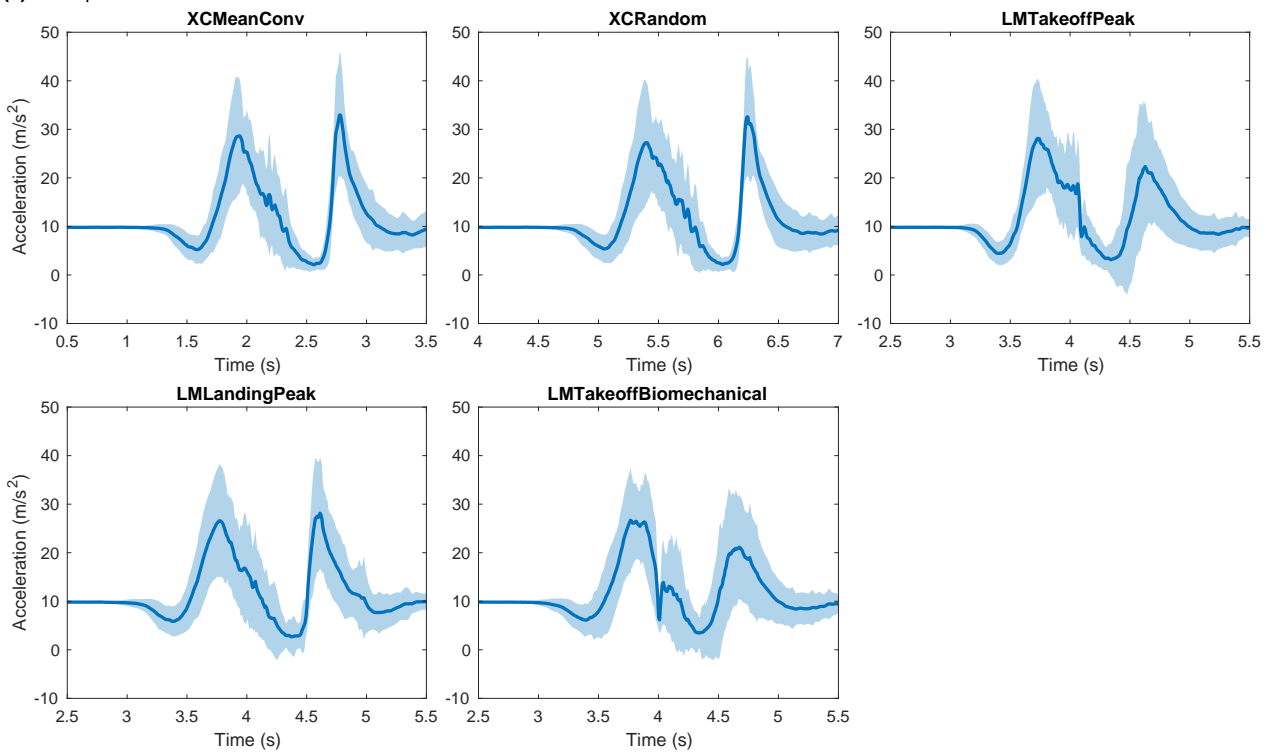
A visual inspection of the Accelerometer signals shows that both cross-correlation methods (XCMeanConv and XCRandom) achieved a high degree of alignment (Figure A1). The cross-correlation methods aligned the signals at the high amplitude peak upon landing. This peak was better resolved than when using the LMLandingPeak method, which identified this peak specifically as the chosen landmark. The landmark methods generally resulted in smaller shared regions at takeoff, but at the expense of larger variation during and after landing, particularly so for LMTakeoffBiomechanical. As a result, the mean curve revealed greater complexity, which had been otherwise averaged out in the landing-focused methods.

The cross-correlation methods for the Smartphone dataset were not as effective, as indicated by larger shaded regions (variance) than the corresponding regions for the Accelerometer dataset. XCMeanConv aligned the signals at or around takeoff, and similarly for XCRandom. The landmark methods tended to leave larger variance regions across the waveform, although LMTakeoffBiomechanical yielded slightly smaller regions. The difference in landmark position between LMTakeoffPeak resulted in slightly different emphasis.

The signal alignment metrics provided a more objective assessment of the signal alignment (Figure A2). XCMeanConv was best for both datasets, achieving the lowest alignment RMSE and the highest Pearson correlation and SNR. When referring back to the alignment plots, SNR appears for the most part to reflect the visual inspection: a high SNR corresponds to tightly aligned signals in Figure A1. LMTakeoffActual performed poorly across these metrics despite being the takeoff time's ground truth measure. Finally, the similarity in the alignment metrics between training and validation sets showed that the reference signals (cross-correlation methods) or reference points (landmark methods) determined from the training set could be applied equally to validation (Appendix A.2).

The choice of alignment method modified the shape of the FPCs, as expected. However, the extent of the change was such that in some cases, a different interpretation of the components was merited (Figure A3). The differences were most apparent for the Accelerometer dataset, between LMTakeoffPeak and XCMeanConv, representing alignment at takeoff or landing, respectively. FPC1 for XCMeanConv captured the variation in acceleration most prominently in the braking phase when acceleration rises before takeoff. In comparison, FPC1 for LMTakeoffPeak captured primarily the variation in flight duration, given that the rise in acceleration on landing occurs later for higher FPC1 scores. An analogy can be drawn using VGRF data in the CMJ to help interpret these components. Higher FPC1 scores for XCMeanConv would be indicative of higher and greater VGRF generation in the braking phase, whereas FPC1 scores for LMLandingPeak signify higher jumps and, by implication, greater peak power. FPC2 for XCMeanConv captured the variation in the amplitude of the acceleration spike on impact, whereas FPC2 for LMLandingPeak had no discernible characteristics in this plot as the component varies so much between subsamples.

(a) Smartphone Dataset



(b) Accelerometer Dataset

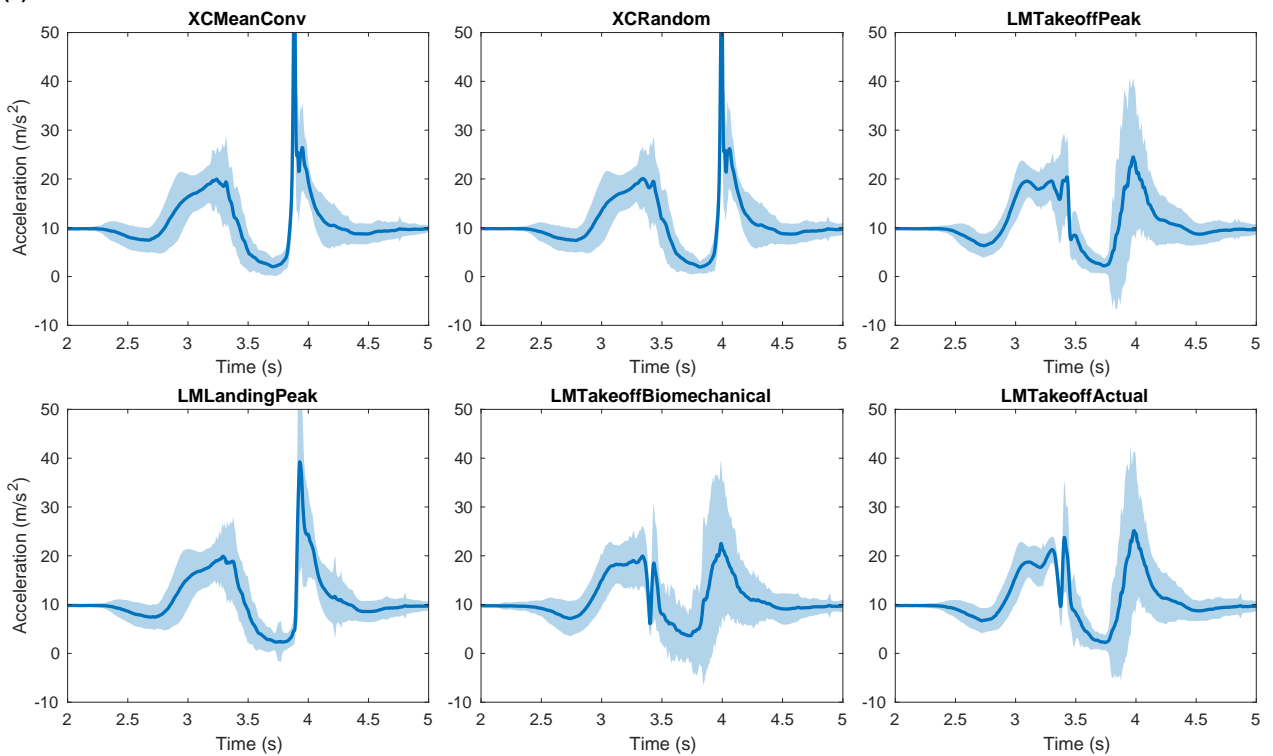


Figure A1. Signal alignments (a prerequisite for FPCA) for the whole dataset, according to different alignment methods. Solid line: mean signal after alignment; shaded region: corresponding standard deviation. A narrow region indicates close alignment. The acceleration rises to a peak immediately before takeoff, then drops towards zero during flight, and then spikes to a high value at landing impact. **LMTakeoffActual** is the ground truth takeoff according to the force plate (Accelerometer only).

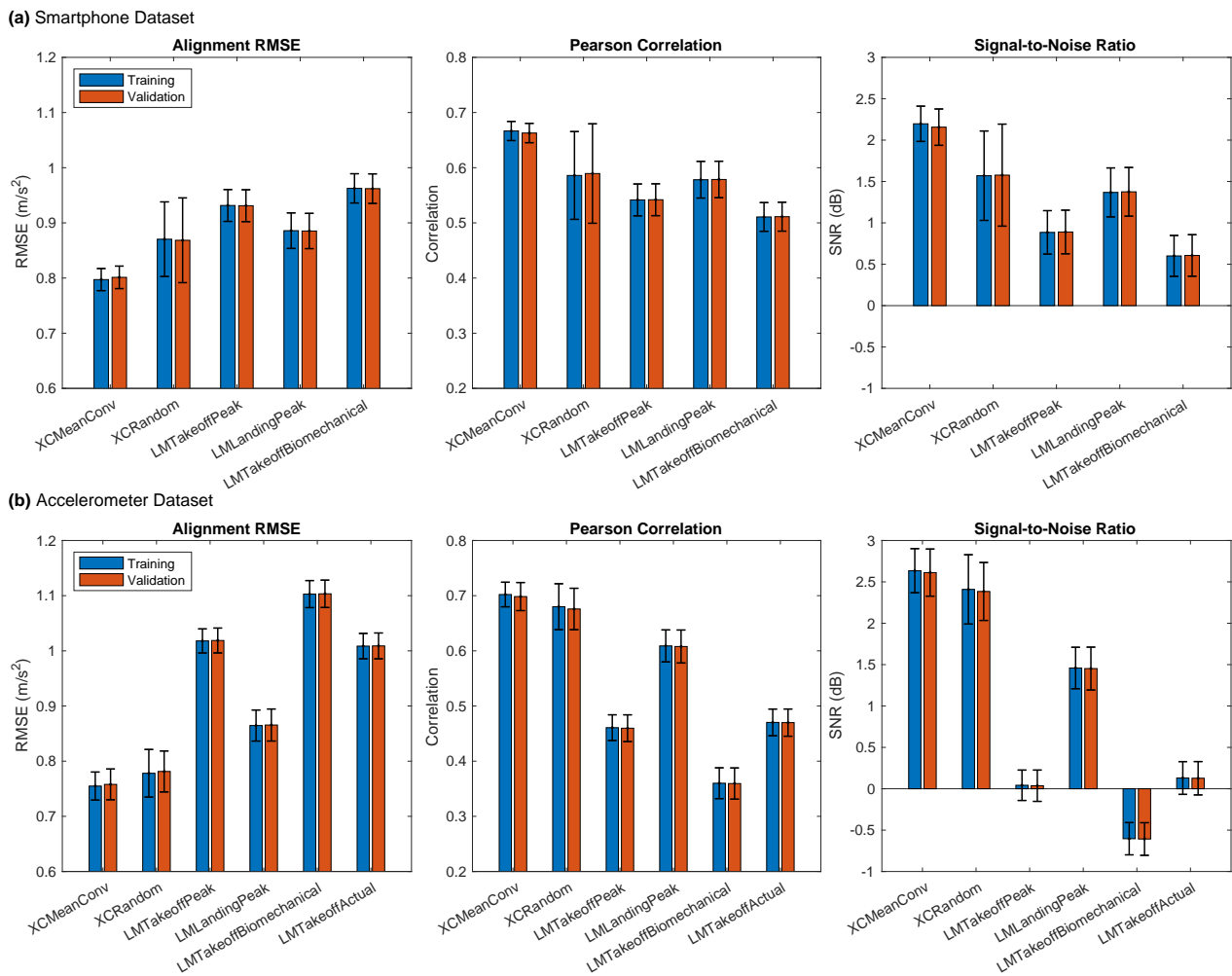


Figure A2. Metrics evaluating the quality of signal alignment achieved by the alignment methods averaged over 50 model fits (25×2 -fold CV). Alignment RMSE is the difference in magnitude between pairs of signals, standardized to z-scores, averaged across their full length (lower is better); Pearson Correlation is the linear correlation between signal pairs (higher is better); Signal-to-Noise Ratio is the ratio signal power to noise power, which is defined here as the squared difference between the signal pair (higher is better).

Appendix B.2. Feature Distributions

The continuous features were generally normally distributed, but the many discrete features were not (Figure A4). Several discrete features exhibited long tails and moderate skew, most notably *A* and *e* of those shown in the figure. The continuous features’ distributions were largely unaffected by the choice of alignment method insofar as the Smartphone dataset was concerned. However, the change was more marked for the Accelerometer dataset. Notably, the Accelerometer FPC1 for LMTakeoffPeak had a bimodal distribution.

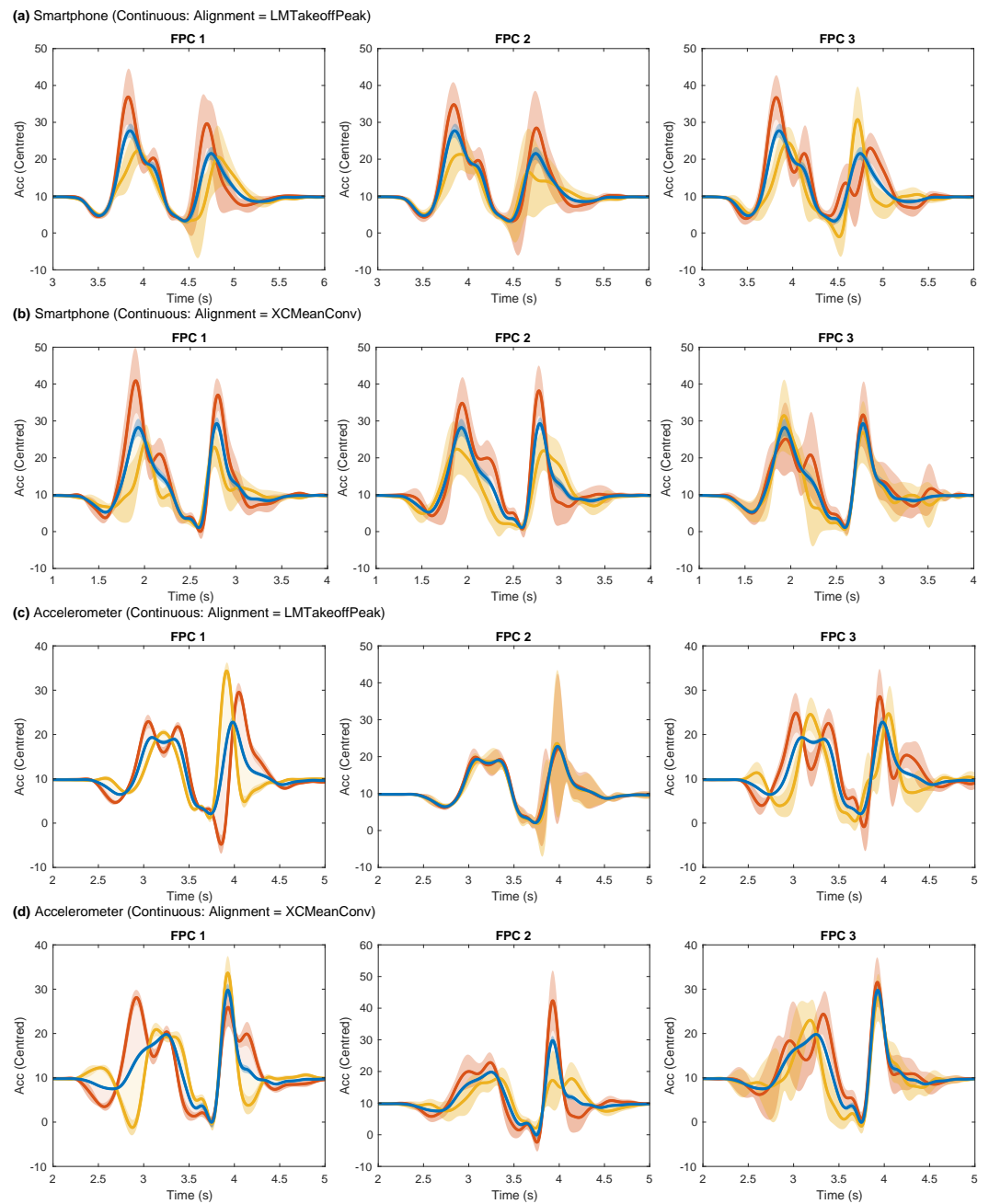


Figure A3. The first three Functional Principal Components (FPCs), respectively, for each dataset based on either the LMTakeoffPeak or XCMeanConv alignment methods. This plot is an adaptation of the traditional FPC plots, showing the modes of variation that arise from changing the corresponding FPC score. The blue line is the mean curve with a score of zero. The yellow line is $-2 \times SD$ of the FPC score, and the red line is $+2 \times SD$. The mode of variation may be imagined by varying the curve from the yellow line through the blue and onto the red line, a transition achieved by increasing the FPC score. The shaded regions for each line represent one standard deviation across subsamples.

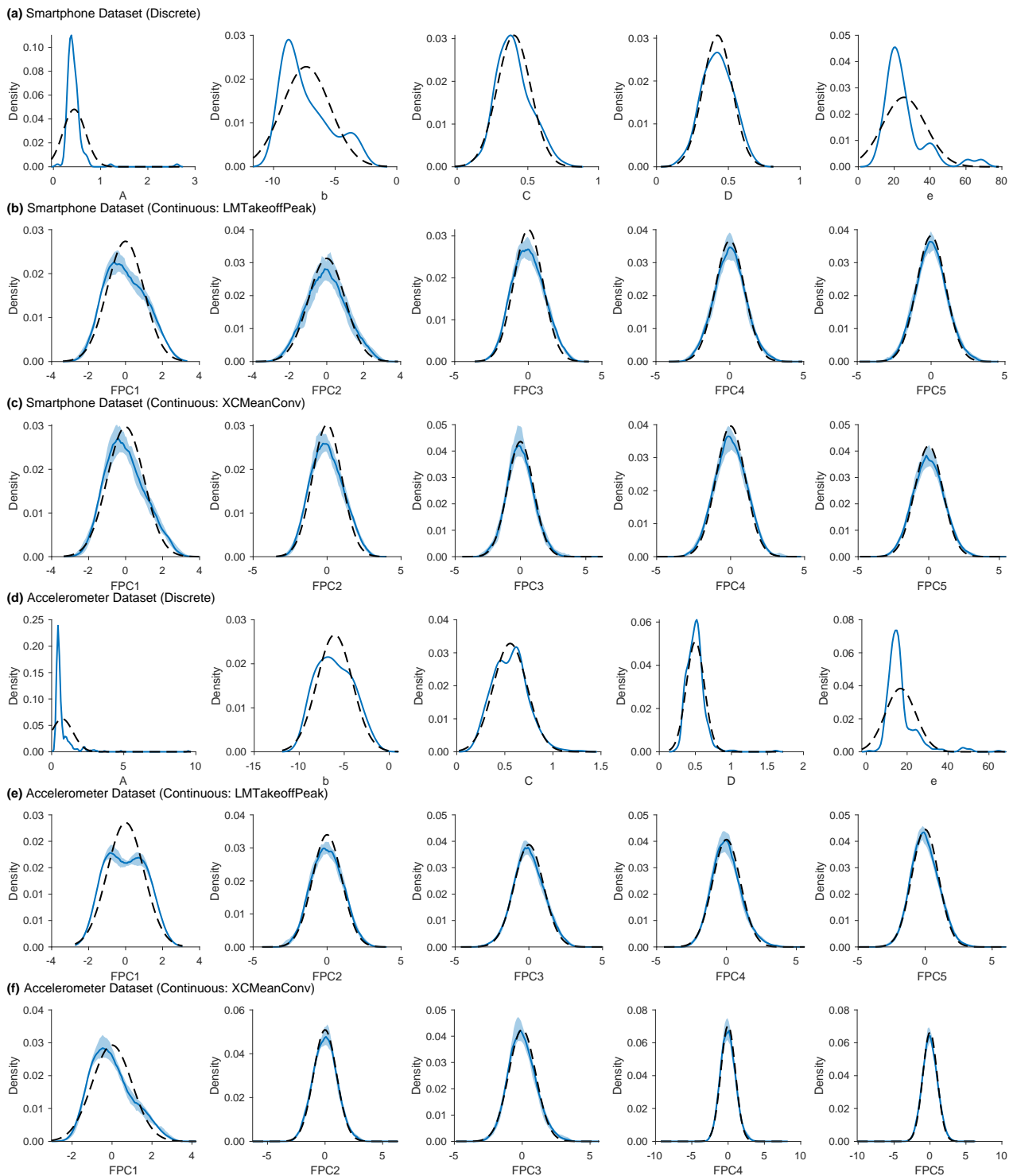


Figure A4. Selected features' probability density distributions before centering, based on the full datasets (solid blue line) compared to the equivalent normal distribution computed from the data's mean and standard deviation (dashed black line). The continuous features have an additional shaded light blue region showing the standard deviation in the distribution between cross-validated folds. Alignment based on the takeoff landmark identified by the algorithm.

Appendix B.3. Linear Model Beta Coefficients

The standardized beta coefficients of the linear model varied between subsamples, reflecting the features' varying degrees of influence (Figure A5). In most cases, the features' direction of influence on the outcome variable could change, either increasing or decreasing

peak power depending on the sign. The variance in continuous features’ beta coefficients in the linear was more consistent across subsamples than those of the discrete features. Indeed, beta coefficients for the same discrete features varied much more than those of the continuous features. This phenomenon was much more prevalent for discrete features, especially for *A*, *G*, *J*, and *M* from both datasets, which can have extreme values, $|\beta| \gg 1$. Hence, the true influence of discrete features on the outcome variable was uncertain.

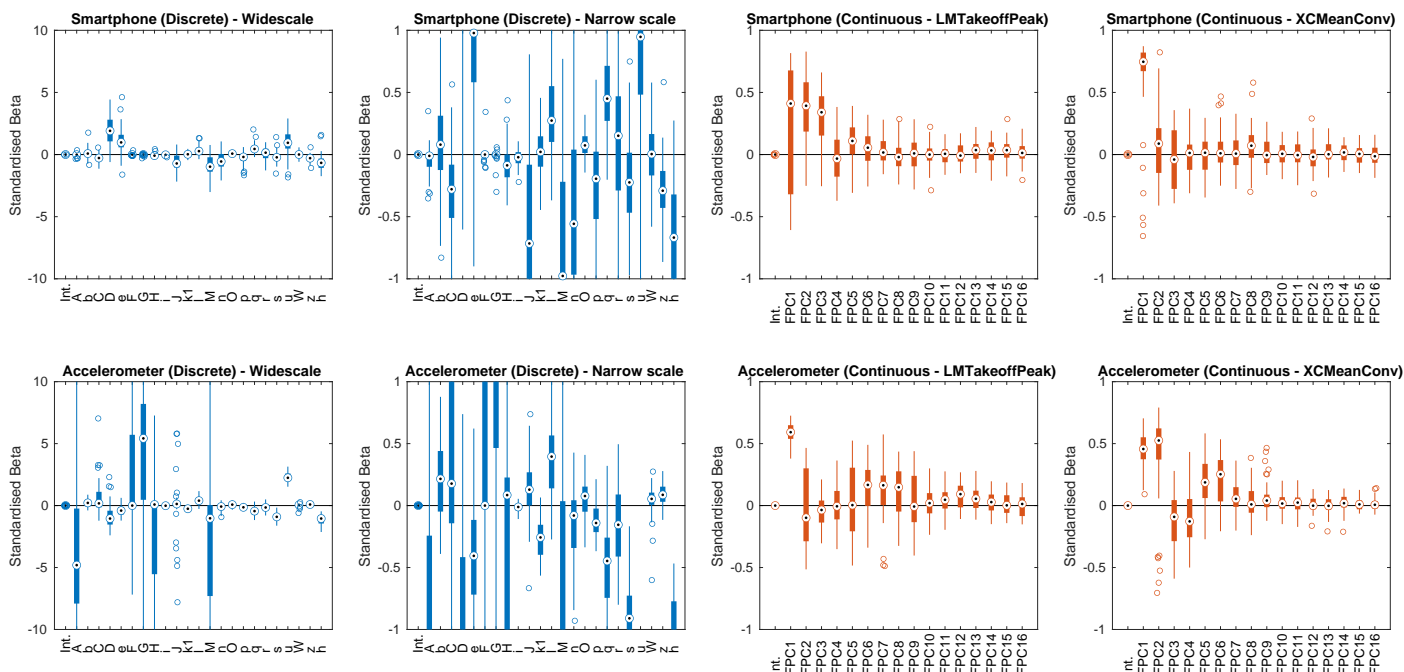


Figure A5. Variance in the linear model’s standardized beta coefficients across 50 model fits (25 × 2-fold CV). The two left-hand columns show betas for discrete features for the same model on two different scales because they vary so much in magnitude. The right-hand two columns show beta for continuous features based on two different alignment methods. A solid bar represents the interquartile range where the small target circle is the median. Passing through the zero line indicates that the predictor can have opposing effects between samples. A standardized beta coefficient of 1 indicates that one standard deviation in the predictor causes one standard deviation in the outcome variable.

References

1. Seshadri, D.R.; Drummond, C.; Craker, J.; Rowbottom, J.R.; Voos, J.E. Wearable Devices for Sports: New Integrated Technologies Allow Coaches, Physicians, and Trainers to Better Understand the Physical Demands of Athletes in Real time. *IEEE Pulse* **2017**, *8*, 38–43. [\[CrossRef\]](#)
2. Adesida, Y.; Papi, E.; McGregor, A.H. Exploring the Role of Wearable Technology in Sport Kinematics and Kinetics: A Systematic Review. *Sensors* **2019**, *19*, 1597. [\[CrossRef\]](#)
3. Preatoni, E.; Bergamini, E.; Fantozzi, S.; Giraud, L.I.; Orejel Bustos, A.S.; Vannozzi, G.; Camomilla, V. The Use of Wearable Sensors for Preventing, Assessing, and Informing Recovery from Sport-Related Musculoskeletal Injuries: A Systematic Scoping Review. *Sensors* **2022**, *22*, 3225. [\[CrossRef\]](#)
4. Cust, E.E.; Sweeting, A.J.; Ball, K.; Robertson, S. Machine and deep learning for sport-specific movement recognition: A systematic review of model development and performance. *J. Sport. Sci.* **2019**, *37*, 568–600. [\[CrossRef\]](#)
5. Chambers, R.; Gabbett, T.J.; Cole, M.H.; Beard, A. The Use of Wearable Microsensors to Quantify Sport-Specific Movements. *Sport. Med.* **2015**, *45*, 1065–1081. [\[CrossRef\]](#) [\[PubMed\]](#)
6. Ancillao, A.; Tedesco, S.; Barton, J.; O’Flynn, B. Indirect Measurement of Ground Reaction Forces and Moments by Means of Wearable Inertial Sensors: A Systematic Review. *Sensors* **2018**, *18*, 2564. [\[CrossRef\]](#) [\[PubMed\]](#)
7. Johnson, W.; Mian, A.; Robinson, M.A.; Verheul, J.; Lloyd, D.G.; Alderson, J.A. Multidimensional ground reaction forces and moments from wearable sensor accelerations via deep learning. *arXiv* **2019**, arXiv:1903.07221v3.
8. Hughes, G.T.; Camomilla, V.; Vanwanseele, B.; Harrison, A.J.; Fong, D.T.; Bradshaw, E.J. Novel technology in sports biomechanics: Some words of caution. *Sport. Biomech.* **2024**, *23*, 393–401. [\[CrossRef\]](#) [\[PubMed\]](#)

9. Dorschky, E.; Camomilla, V.; Davis, J.; Federolf, P.; Reenalda, J.; Koelewijn, A.D. Perspective on “in the wild” movement analysis using machine learning. *Hum. Mov. Sci.* **2023**, *87*, 103042. [[CrossRef](#)]
10. Dowling, J.J.; Vamos, L. Identification of Kinetic and Temporal Factors Related to Vertical Jump Performance. *J. Appl. Biomech.* **1993**, *9*, 95–110. [[CrossRef](#)]
11. Oddsson, L. What Factors Determine Vertical Jumping Height? In *Biomechanics in Sports V*; Tsarouchas, L., Ed.; Hellenic Sports Research Institute: Athens, Greece, 1989; pp. 393–401.
12. Donoghue, O.A.; Harrison, A.J.; Coffey, N.; Hayes, K. Functional Data Analysis of Running Kinematics in Chronic Achilles Tendon Injury. *Med. Sci. Sport. Exerc.* **2008**, *40*, 1323–1335. [[CrossRef](#)] [[PubMed](#)]
13. Ryan, W.; Harrison, A.J.; Hayes, K. Functional data analysis of knee joint kinematics in the vertical jump. *Sport. Biomech.* **2006**, *5*, 121–138. [[CrossRef](#)] [[PubMed](#)]
14. Warmenhoven, J.; Cobley, S.; Draper, C.; Harrison, A.J.; Bargary, N.; Smith, R. Considerations for the use of functional principal components analysis in sports biomechanics: Examples from on-water rowing. *Sport. Biomech.* **2017**, *18*, 317–341. [[CrossRef](#)]
15. Richter, C.; O'Connor, N.E.; Marshall, B.; Moran, K. Analysis of Characterizing Phases on Waveforms: An Application to Vertical Jumps. *J. Appl. Biomech.* **2014**, *30*, 316–321. [[CrossRef](#)] [[PubMed](#)]
16. Halilaj, E.; Rajagopal, A.; Fiterau, M.; Hicks, J.L.; Hastie, T.J.; Delp, S.L. Machine learning in human movement biomechanics: Best practices, common pitfalls, and new opportunities. *J. Biomech.* **2018**, *81*, 1–11. [[CrossRef](#)]
17. Rantalainen, T.; Finni, T.; Walker, S. Jump height from inertial recordings: A tutorial for a sports scientist. *Scand. J. Med. Sci. Sport.* **2020**, *30*, 38–45. [[CrossRef](#)] [[PubMed](#)]
18. Claudino, J.G.; Cronin, J.; Mezêncio, B.; McMaster, D.T.; McGuigan, M.; Tricoli, V.; Amadio, A.C.; Serrão, J.C. The countermovement jump to monitor neuromuscular status: A meta-analysis. *J. Sci. Med. Sport* **2017**, *20*, 397–402. [[CrossRef](#)] [[PubMed](#)]
19. McMahon, J.J.; Suchomel, T.J.; Lake, J.P.; Comfort, P. Understanding the Key Phases of the Countermovement Jump Force-Time Curve. *Strength Cond. J.* **2018**, *40*, 96–106. [[CrossRef](#)]
20. Mascia, G.; De Lazzari, B.; Camomilla, V. Machine learning aided jump height estimate democratization through smartphone measures. *Front. Sport. Act. Living* **2023**, *5*, 1112739. [[CrossRef](#)]
21. White, M.G.E.; Bezodis, N.E.; Neville, J.; Summers, H.; Rees, P. Determining jumping performance from a single body-worn accelerometer using machine learning. *PLoS ONE* **2022**, *17*, e0263846. [[CrossRef](#)]
22. Jones, T.; Smith, A.; Macnaughton, L.S.; French, D.N. Strength and Conditioning and Concurrent Training Practices in Elite Rugby Union. *J. Strength Cond. Res.* **2016**, *30*, 3354–3366. [[CrossRef](#)] [[PubMed](#)]
23. Cormack, S.J.; Newton, R.U.; McGuigan, M.R. Neuromuscular and Endocrine Responses of Elite Players to an Australian Rules Football Match. *Int. J. Sport. Physiol. Perform.* **2008**, *3*, 359–374. [[CrossRef](#)] [[PubMed](#)]
24. Cronin, J.; Hansen, K.T. Strength and power predictors of sports speed. *J. Strength Cond. Res.* **2005**, *19*, 349–357. [[CrossRef](#)]
25. Owen, N.J.; Watkins, J.; Kilduff, L.P.; Bevan, H.R.; Bennett, M.A. Development of a Criterion Method to Determine Peak Mechanical Power Output in a Countermovement Jump. *J. Strength Cond. Res.* **2014**, *28*, 1552–1558. [[CrossRef](#)] [[PubMed](#)]
26. Dragomiretskiy, K.; Zosso, D. Variational Mode Decomposition. *IEEE Trans. Signal Process.* **2014**, *62*, 531–544. [[CrossRef](#)]
27. Ramsay, J.O.; Silverman, B.W. *Functional Data Analysis*, 2nd ed.; Springer Series in Statistics; Springer: New York, NY, USA, 2005.
28. White, M.G.E.; Neville, J.; Rees, P.; Summers, H.; Bezodis, N. The effects of curve registration on linear models of jump performance and classification based on vertical ground reaction forces. *J. Biomech.* **2022**, *140*, 111167. [[CrossRef](#)] [[PubMed](#)]
29. White, M.G.E. Generalisable FPCA-Based Models for Predicting Peak Power in Vertical Jumping Using Accelerometer Data. Ph.D. Thesis, Swansea University, Swansea, UK, 2021.
30. Kutner, M.H.; Nachtsheim, C.J.; Neter, J.; Li, W. *Applied Linear Statistical Models*, 5th ed.; McGraw-Hill/Irwin: Boston, MA, USA, 2005.
31. Tibshirani, R. Regression Shrinkage and Selection Via the Lasso. *J. R. Stat. Soc. Ser. B* **1996**, *58*, 267–288. [[CrossRef](#)]
32. Smola, A.J.; Schölkopf, B. A tutorial on support vector regression. *Stat. Comput.* **2004**, *14*, 199–222. [[CrossRef](#)]
33. Chen, T.; Guestrin, C. XGBoost: A Scalable Tree Boosting System. In Proceedings of the 22nd ACM SIGKDD International Conference on Knowledge Discovery and Data Mining, San Francisco, CA, USA, 13–17 August 2016; pp. 785–794. [[CrossRef](#)]
34. Nielsen, D. Tree Boosting with XGBoost-Why Does XGBoost Win “Every” Machine Learning Competition? Master’s Thesis, Norwegian University of Science and Technology, Trondheim, Norway, 2016.
35. Shao, J. Linear Model Selection by Cross-validation. *J. Am. Stat. Assoc.* **1993**, *88*, 486–494. [[CrossRef](#)]
36. Cawley, G.C.; Talbot, N.L.C. On Over-fitting in Model Selection and Subsequent Selection Bias in Performance Evaluation. *J. Mach. Learn. Res.* **2010**, *11*, 2079–2107.
37. Vabalas, A.; Gowen, E.; Poliakoff, E.; Casson, A.J. Machine learning algorithm validation with a limited sample size. *PLoS ONE* **2019**, *14*, e0224365. [[CrossRef](#)] [[PubMed](#)]
38. Harrison, A.; Ryan, W.; Hayes, K. Functional data analysis of joint coordination in the development of vertical jump performance. *Sport. Biomech.* **2007**, *6*, 199–214. [[CrossRef](#)] [[PubMed](#)]
39. Moudy, S.; Richter, C.; Strike, S. Landmark registering waveform data improves the ability to predict performance measures. *J. Biomech.* **2018**, *78*, 109–117. [[CrossRef](#)] [[PubMed](#)]
40. Hastie, T.; Tibshirani, R.; Friedman, J.H. *The Elements of Statistical Learning: Data Mining, Inference, and Prediction*, 2nd ed.; Springer Series in Statistics; Springer: New York, NY, USA, 2009.

41. Lundberg, S.; Lee, S.I. A Unified Approach to Interpreting Model Predictions. *arXiv* **2017**, arXiv:1705.07874.
42. Ribeiro, M.T.; Singh, S.; Guestrin, C. “Why Should I Trust You?”: Explaining the Predictions of Any Classifier. *arXiv* **2016**, arXiv:1602.04938.
43. Kumar, I.E.; Venkatasubramanian, S.; Scheidegger, C.; Friedler, S. Problems with Shapley-value-based explanations as feature importance measures. In Proceedings of the 37th International Conference on Machine Learning, Virtual, 13–18 July 2020; Volume 119, pp. 5491–5500.
44. Slack, D.; Hilgard, S.; Jia, E.; Singh, S.; Lakkaraju, H. Fooling LIME and SHAP: Adversarial Attacks on Post hoc Explanation Methods. In Proceedings of the AAAI/ACM Conference on AI, Ethics, and Society, New York, NY, USA, 7–9 February 2020; pp. 180–186. [[CrossRef](#)]

Disclaimer/Publisher’s Note: The statements, opinions and data contained in all publications are solely those of the individual author(s) and contributor(s) and not of MDPI and/or the editor(s). MDPI and/or the editor(s) disclaim responsibility for any injury to people or property resulting from any ideas, methods, instructions or products referred to in the content.